Journal of Wind Engineering & Industrial Aerodynamics 226 (2022) 105046

Contents lists available at ScienceDirect

Journal of Wind Engineering & Industrial Aerodynamics

journal homepage: www.elsevier.com/locate/jweia

Calculating gas emissions from open-pit mines using inverse dispersion modelling: A numerical evaluation using CALPUFF and CFD-LS

Seyedahmad Kia [a], Thomas K. Flesch [b], Brian S. Freeman [c], Amir A. Aliabadi [a,*]

[a] School of Engineering, University of Guelph, Guelph, ON, Canada
[b] Department of Earth and Atmospheric Sciences, University of Alberta, Edmonton, AB, Canada
[c] Lakes Environmental, Waterloo, ON, Canada

ARTICLE INFO

Keywords:
Atmospheric transport
CALifornia PUFF (CALPUFF) model
Computational fluid dynamics (CFD) model
Lagrangian stochastic (LS) model
Open-pit mines
Thermal stability

ABSTRACT

Inverse Dispersion Modelling (IDM) establishes a relationship between an air pollutant concentration downstream of a source and the strength of an emission source by reliance on an air dispersion model. Thus, ideally measuring pollutant concentration downstream is sufficient to infer the emission source strength. However, the accuracy of IDM relies on the accuracy of the underlying air dispersion model. Diagnostic dispersion models face difficulty when applied to complex terrains of open-pit mines. To elucidate such difficulties and their causes, the diagnostic CALifornia PUFF (CALPUFF) model is compared to a Computational Fluid Dynamics-Lagrangian Stochastic (CFD-LS) model for quantifying the short-range dispersion of fugitive gases released from a synthetic open-pit mine. Two mine depths (100–500 m) and three thermal stability conditions (stable-neutral-unstable) are investigated. In all cases the surface concentration predicted by the two models are in disagreement, regardless of CALPUFF model setup. Overall, less than 30% of receptor points predict the concentration within a factor of two of CFD-LS simulations ($FAC2 < 0.3$). Model differences appear to be related to the internal algorithms of the CALPUFF model to predict the wind field appropriately. The results should caution practitioners considering diagnostic models for IDM analysis over complex terrain.

1. Introduction

Open-pit mines are used to extract mineral deposits that are close to the earth surface. Mine pits can be spatially large with depths ranging from shallow (few tens of meters) to deep (few hundred meters). Oil sand mines, for example, typically have depths of less than 100 m. Deeper pits can be used in coal mining and hard rock mining for ores such as copper, gold, iron, aluminum, and many other minerals. Mines can be large sources of gases or particulates emissions to the atmosphere (Peng and Lu, 1995), and quantification of their emission rates is an important problem, as it may be needed to meet regulatory requirements, understand the management and mitigation of emissions, or prioritize mitigation efforts.

Quantifying emissions from open-pit mines is a serious challenge for traditional measurement techniques. Flux chambers (FCs) are a simple but intrusive means of measuring gas emissions. One of the difficulties with FC measurements is their spatially small measurement footprint, as well as their impracticality for measuring emissions from vertical surfaces (e.g., mine faces). Micrometeorological approaches, such as eddy-covariance or flux gradient, overcome some of the weaknesses of FCs (e.g., no interference with the emitting surface, larger measurement footprint, capability for long-term monitoring), but they are fundamentally challenged by complex wind conditions, and the difficulty of interpreting their measurements for spatially inhomogeneous emission sources (Meyers et al., 1996; Foken et al., 2012; You et al., 2021).

The Inverse Dispersion Modelling (IDM) approach is a flexible micrometeorological technique having fewer restrictions than other approaches. In the IDM technique, an emission rate is calculated from gas or particulate concentration measured downwind of the source, and an atmospheric dispersion model is used to deduce the emission rate that best fits the measured concentration. There are many examples of IDM studies, ranging from the small scale (observations at distances <10 m from the source) to the continental scale, from point sources to area and volume sources, from continuous emission sources to time varying sources, and from passive tracers (e.g. non-buoyant gases) to active tracers (e.g. heavy particles) (Wilson et al., 1982; Raupach, 1989; Carter

* Corresponding author.
E-mail address: aliabadi@uoguelph.ca (A.A. Aliabadi).
URL: http://www.aaa-scientists.com (A.A. Aliabadi).

https://doi.org/10.1016/j.jweia.2022.105046
Received 21 August 2021; Received in revised form 20 May 2022; Accepted 20 May 2022

et al., 1993; Seibert, 1999; Aylor and Flesch, 2001). Most IDM applications to estimate industrial emissions are local in scale, with concentration sensors located within a few kilometers of the source, and where the terrain is nominally homogeneous and flat. In these situations, simple short-range dispersion models can be appropriate for IDM calculations.

Given the lack of alternatives to measuring emissions from open-pit mines, there is opportunity for IDM to become a useful approach for emission quantification. But this opportunity depends on accurate dispersion model calculations in open-pit environments. The meteorological patterns within and near these mines can be quite different from flat terrain, with topographically induced flow circulations and shear layers (Clements et al., 2003; Whiteman et al., 2004; Nahian et al., 2020), and atmospheric models are challenged by this complexity (Rotach and Zardi, 2007; Medeiros and Fitzjarrald, 2014, 2015; Ren et al., 2018; Byerlay et al., 2020; Nahian et al., 2020; Nambiar et al., 2020a,b; Kia et al., 2021; Liu et al., 2022). High spatiotemporal resolution modeling that is capable of accounting for terrain can be broadly categorized as prognostic, diagnostic, or hybrid models. Prognostic models solve transport questions at a fundamental level, but they are computationally inefficient. Diagnostic models rely on empirical formulations to simulate transport phenomena more efficiently, but at the cost of reduced accuracy. Hybrid models mix the two paradigms to improve computational efficiency and accuracy simultaneously.

In prognostic models the prediction of the wind field over complex terrain is usually based on the numerical solution of the Navier-Stokes' equations, with a turbulence model or method, or the Euler's equations, with an Atmospheric Boundary Layer (ABL) model to simulate turbulence. Numerous Computational Fluid Dynamics (CFD) models have been developed that employed Reynolds Averaged Navier Stokes (RANS) closure schemes (Kim et al., 2000; Neophytou et al., 2011; Breedt et al., 2018; Joseph et al., 2018; Han et al., 2020; Streichenberger et al., 2021; Zhou et al., 2022) or Very Large Eddy Simulation (VLES) methods (Aliabadi et al., 2018; Xia et al., 2020; Ma and Sun, 2021; Ahmadi-Baloutaki and Aliabadi, 2021; Kia et al., 2021) to simulate turbulent transport. This type of modelling has been used to calculate the wind flow within and around open pit mines (Flores et al., 2014; Kia et al., 2021). While prognostic models provide an avenue for high fidelity modelling of terrain impacts, they are difficult and computationally expensive tools that may not be broadly useable in real-world IDM problems.

Diagnostic models may provide a much more practical IDM tool for open-pit mines. As far as diagnostic models are concerned, the CALifornia PUFF Model (CALPUFF) is an industry standard. It is a multilayer, multi-species, and non-steady-state puff dispersion model that simulates the effects of time- and space-varying meteorological conditions on pollution transport (Scire et al., 2000). CALPUFF has been used to investigate dispersion from open-pit mines (Arregocés et al., 2016). The ability of CALPUFF to account for complex terrain relies on CALMET's (CALifornia METeorological) representation of wind complexity. CALMET is a diagnostic model that generates a grid of mass-consistent wind fields. It does not solve the equations of motion. This is a dramatically simpler approach to incorporating flow complexity, and a more likely means of enabling IDM for open-pit mines.

We conducted a "synthetic" modelling study of wind and gas dispersion to examine the potential of a CALPUFF-based IDM approach to measure emissions from an open-pit mine. Our procedure is to use a high-resolution CFD-LS model to represent the "actual" dispersion of gas from a mine, which is then compared against predictions using a CALPUFF simulation. The CFD model has been previously used to model wind flow in open-pit mine environments (Kia et al., 2021), where it accurately represented measured flow fields. Differences between the two models (CALPUFF versus CFD-LS) are used to judge the potential of CALPUFF to provide useful emission rate estimates with IDM. We will examine two open pit mine configurations (shallow and deep), in thermally stable, neutral, and unstable ambient wind conditions. The study is focused on the following questions:

- What are the relative differences in the ground level concentration (downwind of the mine) predicted by the CFD-LS and CALPUFF models?
- How does the CFD-LS and CALPUFF comparison change with different implementations of CALPUFF?
- Does the number and location of the input weather stations for CALPUFF influence the agreement with the CFD-LS simulations?
- Does the agreement between the CFD-LS and CALPUFF predictions of surface gas concentrations downwind of the mine depend on location?

The article is organized as follows. Section 2 describes our methodology. Section 2.1 introduces the open-pit mine characteristics. The details of the CFD model are presented in Section 2.2, and the details of the CALMET and CALPUFF models are presented in Section 2.3. The IDM methodology is described in Section 2.4. The statistical analysis for comparison of the two models is described in Sections 2.5. In Section 3, the results of the simulations for the two types of open-pit mines (shallow and deep) under thermally unstable, neutral, and stable conditions are presented. This includes the visualization of the mine plumes in Section 3.1, the effects of CALPUFF weather and gas receptor station setups on the results in Section 3.2, and the implications in Section 3.3. Section 4 includes the main conclusions and recommendations.

2. Methodology

2.1. Open-pit mine description

Fig. 1 shows the generated shallow and deep kidney-shape mine geometries visualized by CALPUFF View software version 8.6.0. In Table 1 the details of mine walls and dimensions are presented. The generated mine geometry is the same configuration as the geometry of the open-pits of the CFD simulations presented by Kia et al. (2021).

Each mine simulation prescribes five small surface gas sources located around the interior wall of the mine pit (Fig. 2). These might represent five shovel locations digging into the mine face, which release subsurface gas. Each emitting source releases pollutants at a rate of 1 kg s^{-1} from a volume of length, width, and height of 100 m by 100 m by 2 m, with a total emission rate of 5 kg s^{-1} from all sources. All of the sources are located at 50 m and 250 m above the pit's bottom for shallow and deep mines, respectively. The exact location of sources and emission rates (blue squares in Fig. 2) are presented in Table 2.

2.2. Computational Fluid Dynamics and Lagrangian Stochastic (CFD-LS) model

There have been many modeling efforts to understand the turbulence structure of the Atmospheric Boundary Layer (ABL) using various numerical techniques. While Direct Numerical Simulations (DNS) are too computationally expensive and Reynolds-averaged Navier-Stokes (RANS) or eddy viscosity models suffer from lack of accuracy, Large Eddy Simulations (LES) have been used as an effective numerical tool to simulate the ABL with sufficient reliability. In LES, the turbulent eddies of the size of the computational grid cells and larger are explicitly resolved, while the effects of the smaller eddies are parameterized using Sub-Grid Scale (SGS) models. VLES is another powerful tool to economize the CFD simulations. The main distinction between VLES and the standard LES is the determination of filter width with respect to the grid size. In the pure LES, the filter width is associated with the grid size, while the filter width in VLES can be set arbitrarily at any value between the grid size and the large characteristic length scales of the flow. The VLES becomes LES, when the filter width is set as its lowest limit of grid size (Aliabadi et al., 2018; Kia et al., 2021; Ahmadi-Baloutaki and Aliabadi, 2021).

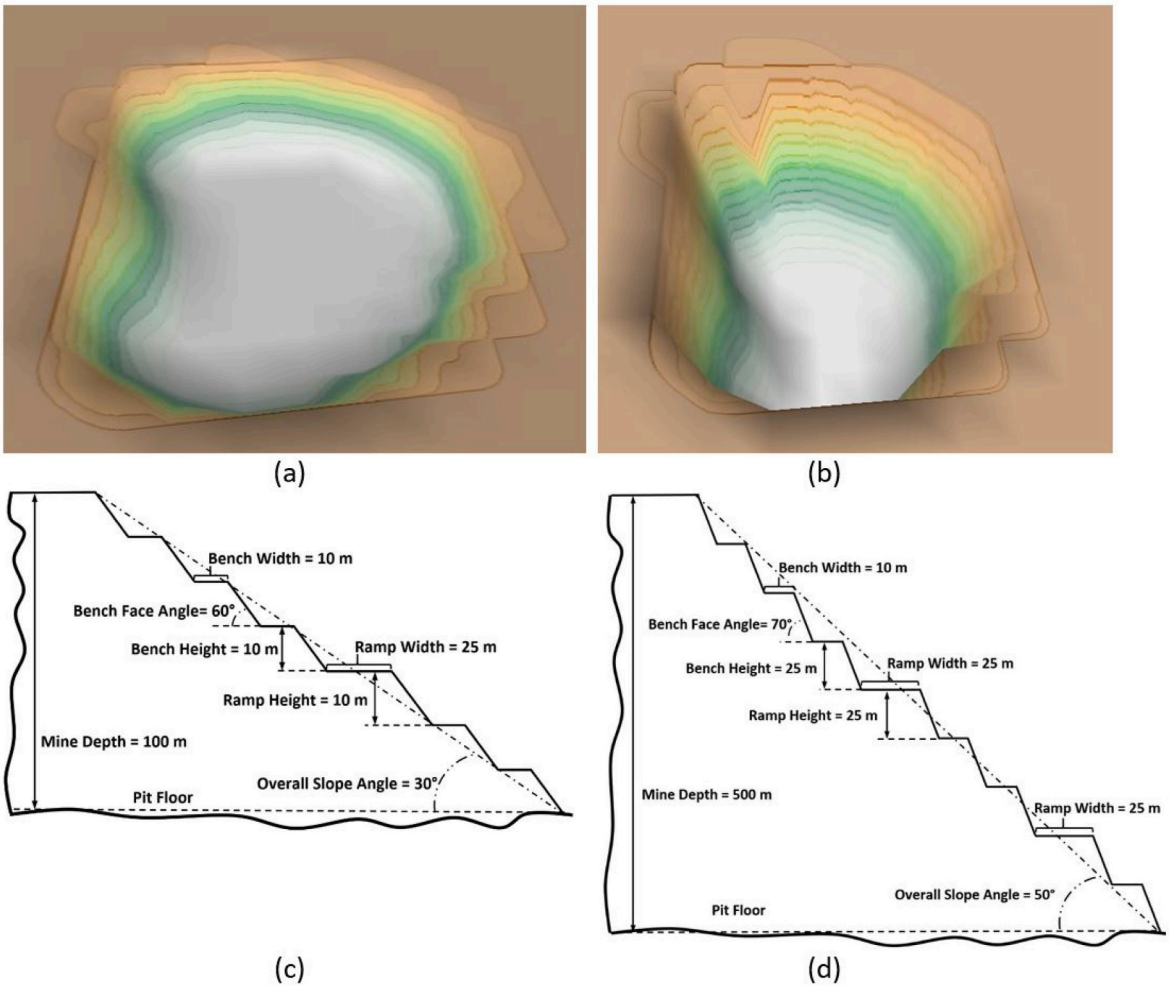

Fig. 1. a) Shallow and b) deep synthetic mine geometries generated by CALPUFF View, c) shallow and d) deep synthetic mine wall details.

Table 1
Dimensions of the stepped shallow and deep mines (Kia et al., 2021).

Geometry	Dimension	
	Shallow Mine	Deep Mine
Overall Slope Angle	30°	50°
Bench Face Angle	60°	70°
Mine Depth	100 m	500 m
Mine Length	1500 m	1500 m
Mine Width	2000 m	2000 m
Bench Height	10 m	25 m
Bench Width	10 m	10 m
Ramp Height	10 m	25 m
Ramp Width	25 m	25 m

In the present paper, the CFD model is based on a VLES method developed by Aliabadi et al. (2018), Ahmadi-Baloutaki and Aliabadi (2021), and Kia et al. (2021). The CFD model is developed for OpenFOAM 4.1. and is used to run the flow field simulations over open-pit mines under different thermal stability conditions and mine depths to simulate atmospheric transport for each configuration. The flow fields from CFD are inserted in the CALPUFF model and an LS model for dispersion simulations.

The CFD domain and boundary identification are shown in Fig. 3. Comprehensive details for the CFD domain were provided by Kia et al. (2021), while a brief description is provided here. For all CFD simulations, the domain length and width are 10000 m and 6000 m, respectively. The mesh discretization in the vertical direction is set to 2 m from the bottom of the mine to 100 m above grade; then it increases to 30 m up to 1000 m above grade; and finally, it is set to 75 m up to the top of the domain. The mesh in the horizontal direction is divided into two sections. First, a very fine mesh is generated surrounding the mine area from $x = 2500$ m to 9000 m that extends to the edges of the mine with a grid spacing of 50 m by 50 m. Second, a coarse mesh is used near the inlet ($x = 0$ m–2500 m) and outlet ($x = 9000$ m–10000 m) of the domain, with a grid spacing of 170 m by 170 m. This mesh is generated to simulate the flow more accurately in the sensitive areas (open-pit mine) and to avoid high computational cost elsewhere. The flow passes over the domain in the stream-wise direction once with a time step of 0.1 s, then the simulations are extended for an additional two flow passes over the domain with a time step of 0.01 s to obtain statistical information by time averaging at a frequency of 10 Hz (Aliabadi et al., 2019, 2021) for 15 min.

For velocity, the synthetic vortex method (Aliabadi et al., 2018) is used at the inlet, the no-slip condition is used at the domain bottom, slip condition is used on the domain top, and the zero-gradient condition is used at the outlet. The mappedField boundary condition (Kia et al., 2021) is used to set the potential temperature profile at the inlet. A spatially-uniform fixed value is used for potential temperature on the bottom surface, and zero gradient condition is used on the top and outlet surfaces. The cyclic boundary condition is assumed for the north and south boundaries for all variables (Kia et al., 2021). The Sub-Grid Scale (SGS) model employed by CFD is known as the oneEqnEddy SGS model in OpenFOAM 4.1 (Aliabadi et al., 2017).

For each simulation a combination of friction velocity and Monin-

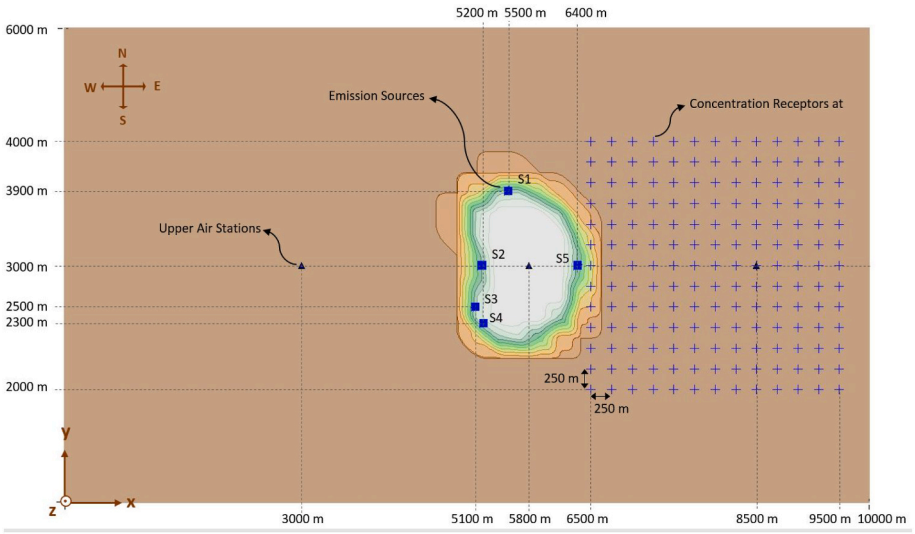

Fig. 2. Location of emission sources, concentration receptors, and upper air stations in the CALPUFF domain.

Table 2
Emission rate and location for the center of emission sources (S1 to S5) for shallow and deep configurations. The z value for shallow and deep configurations are 50 and 250 m from bottom of the pit in the terrain-following coordinate system, respectively.

Sources	Locations (x, y) [m]	Emission Rate [kg s^{-1}]
S1	(5500,3900)	1
S2	(5200,3000)	1
S3	(5100,2500)	1
S4	(5200,2300)	1
S5	(6400,3000)	1

Obukhov length (Table 3) are chosen to determine the thermal stability conditions. The solutions are extracted at 10 terrain following z-levels (10, 15, 25, 40, 65, 100, 200, 300, 500, and 800 m) in a terrain-following coordinate system with a horizontal resolution of 50 m by 50 m. The extracted results in the mentioned levels are the horizontal and vertical mean wind velocity components, some components of Reynolds stresses, and turbulence kinetic energy dissipation rate. The details of the CFD simulation and the results are presented by Kia et al. (2021).

Gas dispersion is calculated from the CFD flow fields using a Lagrangian Stochastic (LS) model. The LS model is a common method to perform dispersion modelling over complex terrain (Bahlali et al., 2019). The LS model calculates the x, y, z [m] trajectories of many tracer particles as they travel downwind of the mine emission sources positioned at five locations along the mine wall. This is a first-order model, in which trajectories are calculated by incrementing changes in particle velocities u, v, and w [m s^{-1}] over a model time-step Δt [s]. The LS model details are described by Wilson et al. (2009, 2010) and only a brief

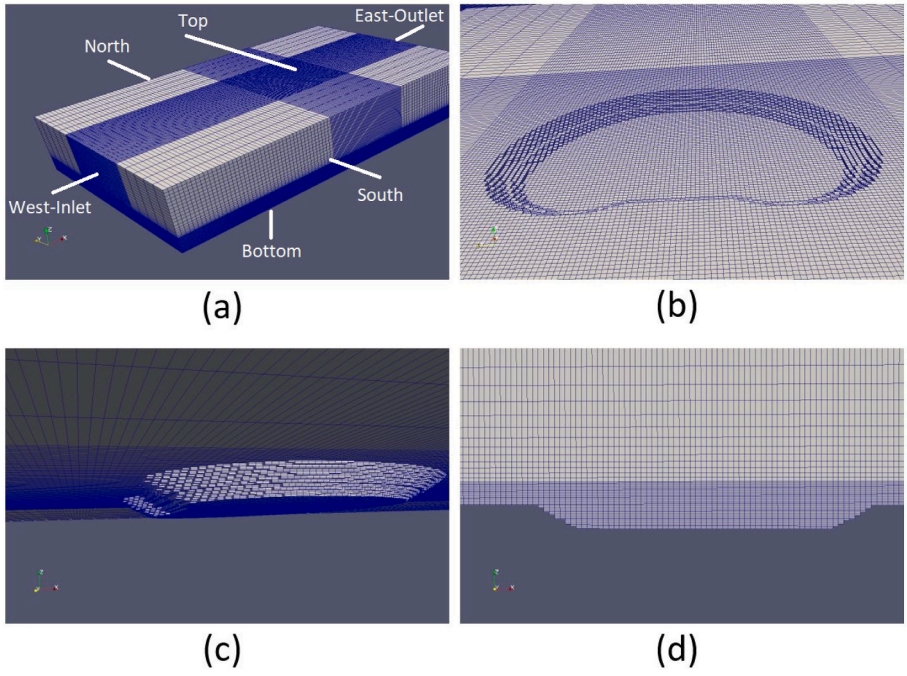

Fig. 3. Generated CFD mesh and boundary identification for the shallow mine, a) view of domain and boundary conditions, b) view of mine from above grade, c) view of mine from below grade, and d) view of mine cross-section.

Table 3
Friction velocity and Obukhov length upwind of the mine for shallow and deep mine configurations; data reported under various thermal stability conditions.

Mine Type	Symbol	Value
Thermally unstable		
Shallow	$u_{*,10\ m}$ [m s^{-1}]	0.29
	$L_{10\ m}$ [m]	−11.60
Deep	$u_{*,10\ m}$ [m s^{-1}]	0.33
	$L_{10\ m}$ [m]	−27.18
Thermally neutral		
Shallow	$u_{*,10\ m}$ [m s^{-1}]	0.46
	$L_{10\ m}$ [m]	–
Deep	$u_{*,10\ m}$ [m s^{-1}]	0.52
	$L_{10\ m}$ [m]	–
Thermally stable		
Shallow	$u_{*,10\ m}$ [m s^{-1}]	0.26
	$L_{10\ m}$ [m]	9.36
Deep	$u_{*,10\ m}$ [m s^{-1}]	0.23
	$L_{10\ m}$ [m]	31.45

summary is provided here. The LS model uses gridded flow statistics calculated by the CFD model: the mean velocities in each coordinate, the velocity variances in the three coordinates $\sigma_{u,v,w}$ [m s^{-1}], and the turbulent kinetic energy dissipation rate ε [m^2 s^{-3}]. In our LS simulations the covariance between velocity components are neglected. The LS model time-step is set as a fraction of the effective Lagrangian timescale, calculated as $T_L = 2\sigma_w^2(C_0\varepsilon)^{-1}$, with Δt [s] equal to $0.2T_L$ under unstable and neutral conditions, and $0.02T_L$ under stable condition (the value of C_0 is assumed to be 3.59). As particles move downwind they may cross the ground surface (i.e. taken as the roughness length z_0 [m]), in which case the particles are reflected back into the flow domain.

To represent gas dispersion, 25000 model particles are released randomly over each source (with the footprint described in the previous section). These particles travel away from the source in accordance with the flow field, and eventually move downwind of the mine and exit the model domain. A set of concentration receptors are located downwind of the mine pit (Fig. 2). Each receptor is a volume (Δx, Δy, Δz = 10, 50, 10 m) where the time-average gas concentration is calculated from the residence time of the LS particles within the volume. The number and location of the receptors depend on the problem being investigated.

2.3. CALPUFF

CALPUFF is a transport and dispersion model that advects and diffuses puffs of material emitted from modeled sources, simulating dispersion and transformation processes along the way. CALPUFF's dispersion calculations typically use the three-dimensional wind fields generated by the CALMET model. CALMET is a diagnostic model that generates a grid of mass-consistent wind field using a three-step process. The first step is to interpolate/extrapolate observed wind data to grid points in the modeling domain. The wind field interpolation/extrapolation is based on the inverse square of the weighted distance between the grid points and the wind observations, giving more weight to the nearness of the observation points (Scire et al., 2000). An observation is excluded from interpolation/extrapolation if the distance from the observational station to a particular grid point exceeds a maximum radius of influence. The second-step in generating the gridded wind field uses parameterizations to account for the kinematic effects of terrain, slope flows, and blocking effects. The third step adjusts the wind fields to meet the mass consistency requirement by minimizing the divergence of the flow field.

In the present work, two sets of synthetic mine geometries, namely shallow and deep mines, under three different thermal stability conditions (unstable, neutral, and stable) are simulated by CALPUFF View 8.6.0 (Lakes Software) and CFD-LS models. At the first step, the wind field predicted by CFD (Kia et al., 2021) for each of the six different mine configurations and stability conditions is assumed as the real flow field over the synthetic open-pit mining area to be the input of both the CALPUFF the LS models. The concentration field produced by the CFD-LS model is used for comparison with the CALPUFF plume distribution predictions. The wind field produced by the CFD model is used for comparison with the dataset for the flow field predicted by CALMET.

The mines' upstream edge is located at $x = 5000$ [m] in the streamwise direction. This allows for an adaptation distance such that flow mean and turbulence statistics generated by CFD adopt representative atmospheric conditions before studying transport phenomena over the mines (Aliabadi et al., 2018; Ahmadi-Baloutaki and Aliabadi, 2021; Kia et al., 2021). Table 3 shows the friction velocity u_* [m s^{-1}] and Obukhov length L [m] for the CFD-LS and CALPUFF simulations under the three different thermal stability conditions. These u_* [m s^{-1}] and L [m] values apply to the flow conditions upwind of the mine.

The open-pit mine terrain is generated with CALMET's geophysical processor with the horizontal resolution of 250 m by 250 m with a user-defined land use. The surface roughness is set to be $z_0 = 0.3$ m, appropriate for the modified land within the boreal forest of northern Canada (Raupach et al., 1991; Kia et al., 2021), all over the domain, which creates a uniform aerodynamic roughness for all surfaces. The domain is divided into 11 vertical layers (20, 40, 60, 80, 100, 200, 600, 800, 1000, 1200, and 1300 m above surface). The vertical layers are more dense below 100 m, which is the volume close to the surface. This part of the boundary layer is more important than upper layers for investigation of the plume distribution near the ground. The meteorological and gas sampling grid cells have a horizontal resolution of 250 m by 250 m. The same horizontal resolution is used in the LS simulations. CALPUFF is set to use the properties of methane gas as the pollutant, although hereafter we interpret that gas as broadly representing a neutrally buoyant tracer.

The wind speed, wind direction, potential temperature, and pressure calculated by CFD are used to generate the required data for the surface and upper air stations in CALMET. The wind field data at 10 m and 1300 m above the surface in terrain-following coordinates are extracted from the CFD model to be used as the surface and upper air stations, respectively. No precipitation or cloud cover are assumed in the simulations. For all the six simulations, three upper air stations are considered and located in the terrain-following coordinates at (x [m], y [m], z [m]) of (3000, 3000, 1300)-west station, (5800, 3000, 1300)-mine station, and (8500, 3000, 1300)-east station, which can be seen with blue triangles in Fig. 2. Radius of influence of terrain features, which is a function of the dominant scale of the terrain is suggested by Scire et al. (2000) to be 5 to 10 time of the grid spacings wide and large enough to cover topographical changes in the domain. In the present simulations, as the mines' widths are 2 km and the grid spacing is 250 m, the radius of influence of terrain features is set to be 2 km for all the simulations.

We used 169 discrete concentration receptors at 10 m above the ground placed downstream of the mine (from 6500 m to 9500 m in x-direction and 2000 m–4000 m in y-direction) to record the surface gas concentration for the model comparison purposes (blue pluses in Fig. 2). For the wind field comparison, 26 points outside the mine at 10 m above the surface and 15 points inside the mine at 10 m above the surface are selected (red dots in Fig. 4). Also, two vertical columns of receptors from 10 m above the surface up to the top of the domain are defined at (x = 5800 m, y = 3000 m) and downstream at (x = 8500 m, y = 3000 m) to record data in the vertical direction for the purpose of wind field comparison throughout the depth the ABL (yellow stars in Fig. 4).

The simulations investigate the effects of the number of surface stations on the CALMET-generated wind field and the CALPUFF-generated concentration field. The number of surface stations is changed both inside and outside of the mine, from a high resolution case with 24 and 95 surface stations inside and outside the mine, respectively, to a low resolution case with only one surface station outside the mine. The seven cases with defined surface stations are summarized in Table 4. Case C1 is called the high resolution case as it has the highest

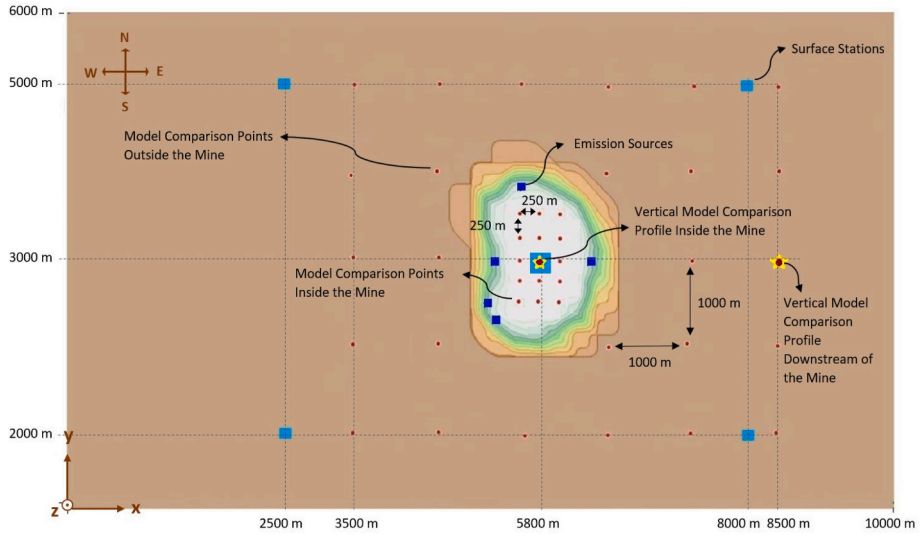

Fig. 4. Arrangement of surface and upper weather stations associated with the operational case C6; location of the model comparison points for wind field modeling using CALPUFF.

number of surface stations inside and outside of the mine, and case C6 is called the operational case as the number of surface stations inside and outside of the mine is seen as being a practical measurement configuration that could be used in a real-world mine study.

The operational case C6 is pursued further to investigate the effects of changing the location of surface stations on the CALPUFF dispersion simulations. For this purpose, the locations of the surface stations outside the mine at upstream and downstream sides are changed in the x-direction for four additional cases. The x-location of the four cases are $x = 1000$, 8000 m, $x = 3000$, 7000 m, $x = 3000$, 8000 m, and $x = 3000$, 9000 m. The results of the simulations are compared with the concentration and wind fields from the CFD-LS results.

The effects of changing the location of concentration receptors outside the mine are studied for the operational case C6. For this purpose, seven arrays of discrete receptors at $x = 6500$, 7000, 7500, 8000, 8500, 9000, and 9500 m (from the east edge of the mine to the end of the computational domain) are selected to compare the concentration at each array with CFD-LS concentration at the same location of receptors at 10 m above surface. All the CALMET and CALPUFF results are presented after 1-h averaging.

2.4. The Inverse Dispersion Modelling paradigm

The specific focus of this study is the use of IDM to calculate mine emissions. The IDM technique is based on the simple idea that when a mine emits gas at an unknown rate Q [kg s^{-1}], the gas concentration downwind of the mine C [μg m^{-3}] will increase above the ambient background concentration C_b [μg m^{-3}], and that a measurement of ($C - C_b$) [μg m^{-3}] indicates Q [kg s^{-1}]. The link between Q [kg s^{-1}] and ($C - C_b$) [μg m^{-3}] is calculated with an atmospheric dispersion model. Given the theoretical ratio $(C/Q)_{\mathrm{Sim}}$ provided by an atmospheric dispersion model and a measurement of ($C - C_b$) [μg m^{-3}], one can infer Q [kg s^{-1}] (Flesch et al., 2005):

$$Q = \frac{(C - C_b)}{(C/Q)_{\mathrm{Sim}}}. \tag{1}$$

Equation (1) is the conceptual format for an IDM calculation. In this study we report C [μg m^{-3}], assuming that $C_b = 0$ [μg m^{-3}]), downwind of a fixed emission source $Q = 5$ [kg s^{-1}]. This is equivalent to reporting the values of $(C/Q)_{\mathrm{Sim}}$ provided by the CFD-LS and the CALPUFF models. The CFD-LS model is assumed to be our best estimate of $(C/Q)_{\mathrm{Sim}}$ for the complex open-pit mine terrain, and we are interested to know how well CALPUFF reproduces the CFD-LS value.

Table 4
The number of surface stations inside and outside the mine for meteorological forcing of the CALMET model.

Case No.	Number of surface stations	
	Inside Mine	Outside Mine
C1 (High Resolution Case)	24	95
C2	24	12
C3	8	4
C4	1	95
C5	1	12
C6 (Operational Case)	1	4
C7	0	1

2.5. Statistical analysis

Quantitative comparisons between the CALPUFF model (M_i) and CFD-LS model (O_i) outputs (concentration and wind speed) are performed by determining the Bias and Root Mean Square Error (RMSE) defined by

$$Bias = \frac{\sum_{i=1}^{n}(M_i - O_i)}{n}, \tag{2}$$

$$RMSE = \sqrt{\frac{\sum_{i=1}^{n}(M_i - O_i)^2}{n}}, \tag{3}$$

where n is the number of data accounted for in the error statistic calculation. Because wind direction is a circular variable, differences of wind direction between CALPUFF and the CFD-LS models are reported as a positive number less than 180° by calculating the Mean Absolute Error (MAE) (instead of Bias) (Nahian et al., 2020) defined by Fernández-González et al. (2018).

$$MAE = \frac{\sum_{i=0}^{n}|M_i - O_i|}{n}. \tag{4}$$

To assess the spatial distribution of the concentration field predicted by CALPUFF, another statistic is used. The fraction of receptor points that predict the concentration within a factor of two of CFD-LS simulations is termed *FAC2* and defined by Hanna et al. (1993) and Wang et al. (2008).

$$FAC2 = \text{fraction of data for which } 0.5 \leq C_M/C_O \leq 2. \quad (5)$$

For modeling of air pollution dispersion over complex terrain (e.g. urban areas), Hanna and Chang (2011) suggest that a model performance in complex urban environments is acceptable if *FAC*2 is greater than about 30%. This is a more relaxed cutoff than suggested for models of dispersion over flat and homogeneous terrain. Here we note that the *FAC*2 statistic for the concentration ratio C_M/C_O is also the *FAC*2 statistic for the ratio of the IDM-calculated emission rates using Equation (1). This is because for a neutrally buoyant and chemically inert tracer, the concentration ratio from the two models (above background concentration) is equal to the emission rate ratio for a given source configuration and atmospheric condition. So the *FAC*2 statistic gives the proportion of receptor points where an IDM calculation using CFD-LS and CALPUFF values of $(C/Q)_{\text{Sim}}$ differ by less than a factor of two. In addition, *FAC*5 and *FAC*10 are computed in this study, but the results are not provided for brevity. These statistical metrics help decide if an air pollution dispersion model provides acceptable results.

3. Results and discussion

In this section we begin by presenting contour plots of gas concentration as estimated from the CALPUFF and CFD-LS models. These plots will show that large differences exist in the concentration plumes as calculated from the two models. We then examine the statistical agreement in concentration and wind field estimates between the two models, and the sensitivity of the statistical metrics to the weather stations and receptor configurations used by CALPUFF. Finally we discuss the implications of these results to the potential of using IDM to calculate the emission rate from open-pit mines.

3.1. Plume visualization for CALPUFF and CFD-LS models

Fig. 5 shows the contour plots of surface gas concentration for the shallow mine under the three thermal stability conditions using CALPUFF case C6 (i.e., the CALPUFF flow field is calculated using wind information from four surface stations outside and one inside the mine). Under the thermally unstable condition, we note that CALPUFF has enhanced the horizontal dispersion of material downwind of the mine relative to CFD-LS. While the CFD-LS simulations suggest three distinct plume "fingers" immediately downwind of the mine (these fingers roughly correspond to the *y*-grouping of the sources), in CALPUFF the individual source plumes quickly merge to a single broad plume. Excess diffusion of the plumes by CALPUFF were elucidated in other studies (Li and Guo, 2006; Tomasi et al., 2019; Toscano et al., 2021). Under thermally neutral conditions, the lateral dispersion of tracer in both CFD-LS and CALPUFF is reduced compared to the unstable conditions. With CALPUFF we now see the three plume fingers downwind of the mine. Under the thermally stable condition, lateral dispersion is reduced even further. The most striking feature in the stable condition is the large area of zero-concentration downwind of the mine in the CFD-LS model results, and the counter-intuitive trend of increasing surface concentration with increasing distance downwind of the mine (over at least part of the domain). This behavior was also seen in the earlier study of Kia et al. (2021), and linked to plume rise from the mine that lifts the plume above the downwind surface, followed by dispersion of the plume back down to the surface with increasing distance.

Fig. 6 shows a vertical slice of the CFD-LS and CALPUFF plumes at a location approximately 500 m downwind of the mine (x = 7000 m). These vertical slices consistently show that CALPUFF simulates a wider plume than does CFD-LS, mirroring what we noted in the horizontal slices in Fig. 5. The CALPUFF plumes are also more dispersed in the vertical direction. Under the thermally unstable condition, the CFD-LS slice shows the three surface level plume fingers noted in Fig. 5 exist

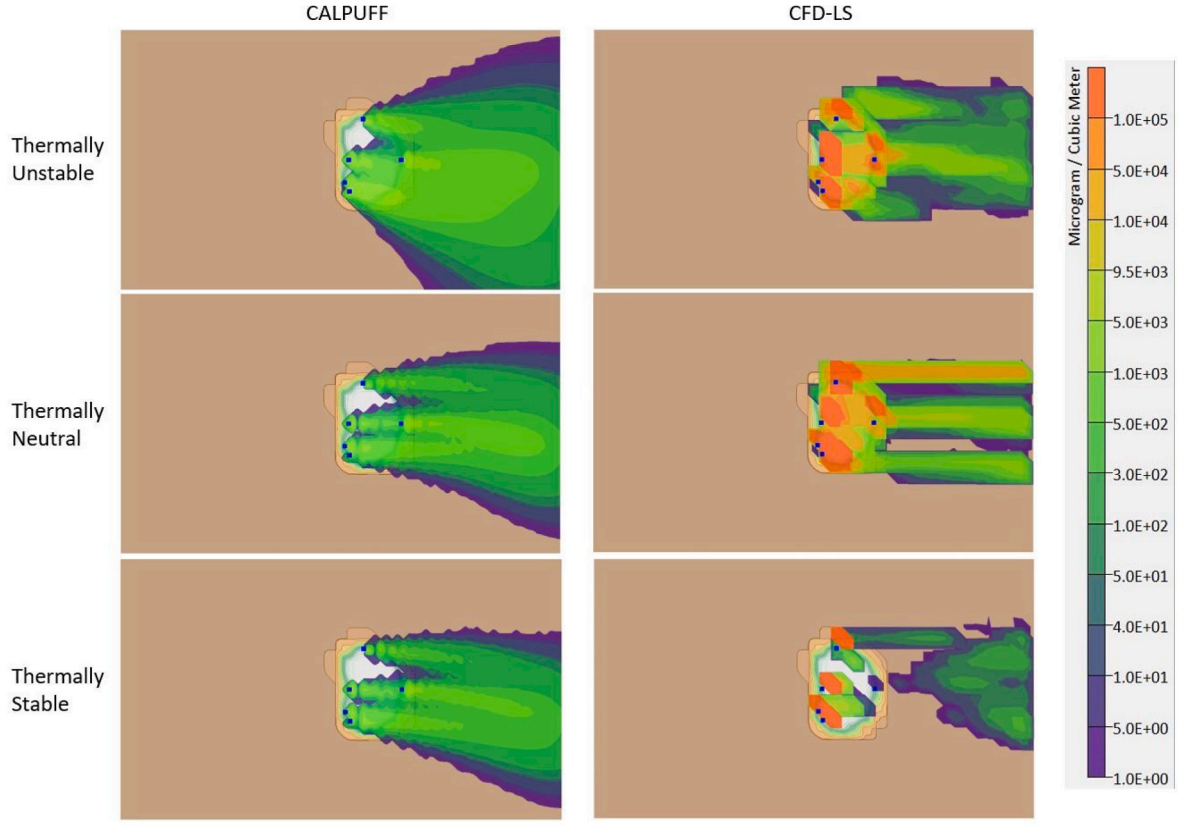

Fig. 5. Contour plots of surface tracer concentration for the shallow mine case, as predicted from CALPUFF case C6 (left) and CFD-LS (right).

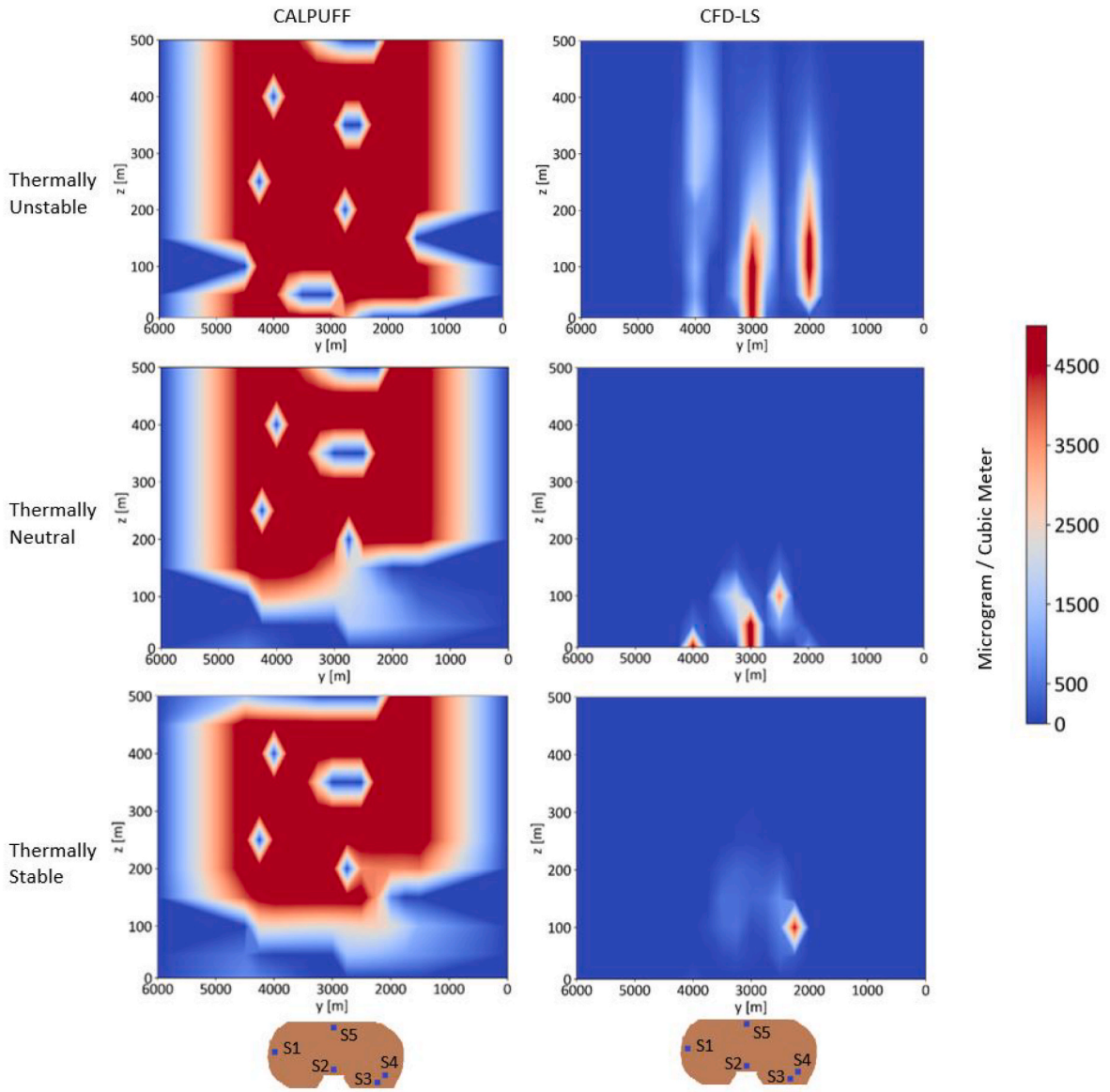

Fig. 6. Contour plots showing a vertical slice of tracer concentration downwind of the shallow mine ($x = 7000$ m), as predicted with CALPUFF case C6 (left) and CFD-LS (right). The distribution of sources in the mine is shown below the plots for reference.

aloft too. It is interesting that two of the three fingers are elevated, having maximum concentration levels above the surface (this would be unexpected for a ground level source in simple terrain). The unstable CALPUFF plume does not replicate these details. The CFD-LS and CALPUFF plumes are particularly different under the thermally stable condition. The CFD-LS plume slice shows a concentrated "filament" centered at $y = 2220$ m, $z = 100$ m, while the CALPUFF plume is dramatically more dispersed.

We speculate that the gas plume from an actual mine pit is likely to be very concentrated and elevated as it passes over the downwind edge of the mine. The elevated plume explains the absence of surface-level gas just downwind of the mine (a concentration "shadow"). From that initial elevation at the mine edge, the plume slowly mixes down to the surface, resulting in an increase in concentration with increasing distance from the mine. This behavior is not seen in the CALPUFF plume.

3.2. Different CALPUFF weather station setups

The flow field used to calculate dispersion in CALPUFF is given by the CALMET model, based on wind information measured at input "weather stations". The number and location of these stations can be chosen by the user, and can have an impact on the CALPUFF predictions. In this section we consider several possible settings of the surface weather stations (Table 4). These cover a range of implementations that could be used in a model application. In the following discussion we assume the CFD-LS model gives the true concentration and wind fields in the various open-pit situations, and we evaluate the impact of the CALMET settings in terms of the statistical agreement between the CALPUFF and CFD-LS concentration and wind fields.

3.2.1. Effect of the number of met stations

Fig. 7 shows the Bias [μg m^{-3}] and RMSE [μg m^{-3}] of the surface gas concentrations calculated by CALPUFF downwind of the mine. One of our hypotheses was that the case having the greatest number of input weather stations ("high resolution" case C1) would provide more accurate CALPUFF predictions (i.e. the best agreement with CFD-LS). Across the two mines and three stability conditions, there was no clear evidence that the high resolution case C1 gave better predictions in terms of Bias [μg m^{-3}]. In terms of RMSE [μg m^{-3}], only in the shallow-mine unstable condition did we find that the higher resolution cases (C1

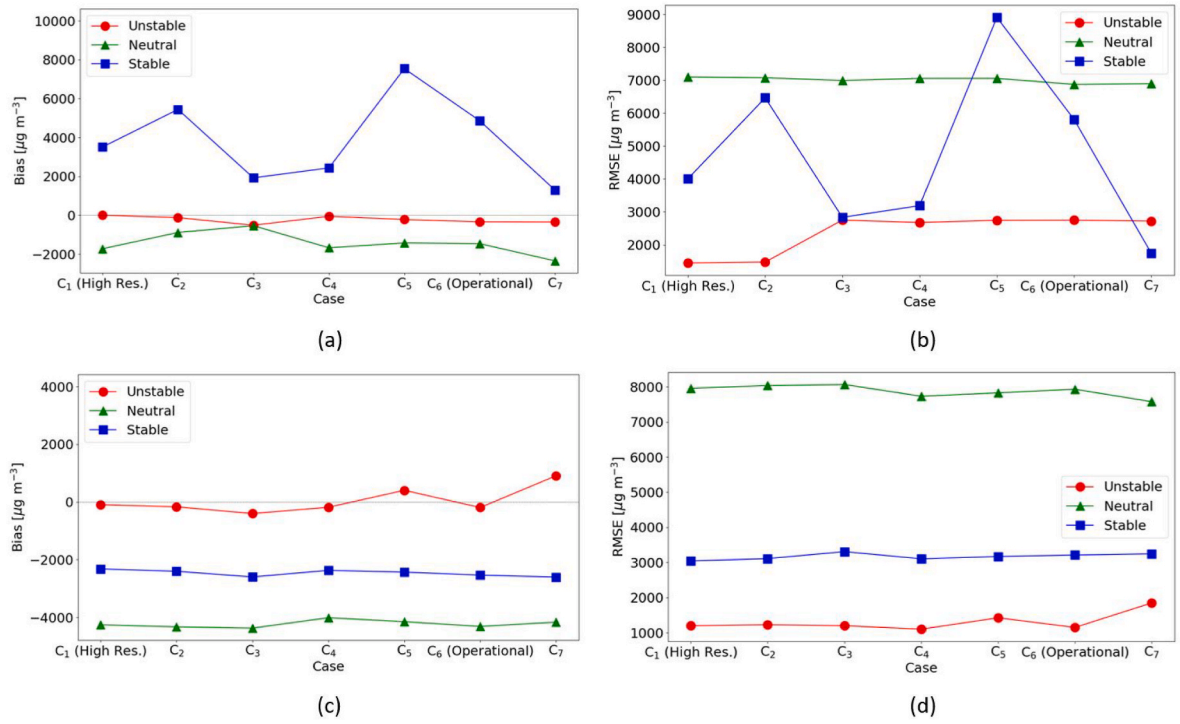

Fig. 7. Bias [$\mu g\ m^{-3}$] and RMSE [$\mu g\ m^{-3}$] of the tracer concentrations outside of the mine, comparing CALPUFF predictions against CFD-LS over the different surface station setting cases and thermal stability conditions of the shallow (a and b) and deep (c and d) mine configurations.

and C2) had lower errors than the other cases. Another hypothesis was that having more weather stations in the mine pit allows a better representation of the flow complexity in CALPUFF, which would result in a better concentration predictions (e.g., case C3 would be better than cases C5 or C6). Having more weather stations in the mine did improve CALPUFF performance in the shallow-mine stable condition, as both the Bias [$\mu g\ m^{-3}$] and RMSE [$\mu g\ m^{-3}$] values of case C3 were better than for cases C4–C6. Earlier we discussed the interesting and counter-intuitive plume characteristics in the shallow-mine under thermally stable condition (elevated and compact plume as it exited the mine), and perhaps this explains why we saw improvement in the performance of CALPUFF when we added more in-mine weather stations in this case. However, in the five other situations, there is little to recommend having more weather stations in the mine. Another hypothesis was that the least accurate CALPUFF predictions would occur when only a single weather station was used (case C7). The most surprising result illustrated in Fig. 7 is that there was no general degradation in CALPUFF performance when only a single weather station is used. Only in the deep mine configuration and under unstable condition did we see a clear decline in performance. In total, we did not observe large sensitivities in CALPUFF performance based on the number of the input weather stations.

Fig. 8 shows the calculated *FAC*2 percentage of receptor concentrations from the various CALPUFF runs. This statistic gives the fraction of receptors (downwind of the mine) where the CALPUFF calculated concentration is within a factor of two of the CFD-LS result. In terms of IDM, this statistic will also give the fraction of receptors where the emission rate estimate from the two models is within a factor of two of each other. The clearest conclusion one can draw from Fig. 8 is that for the large majority of downwind locations, the CALPUFF predictions are more than a factor of two different from CFD-LS. In fact this is also true if we look at *FAC*10 (not shown), in which the majority of receptors have a concentration that is more than a factor of 10 different from CFD-LS. There are two other conclusions we can draw from Fig. 8. In our simulations, the trend was for CALPUFF to overestimate the surface concentrations. Tomasi et al. (2019) compared CALPUFF and LS model predictions for a tracer release study in mountainous terrain. They found a similar trend where CALPUFF overestimated both the LS model calculations and the actual tracer observations. Another conclusion is that

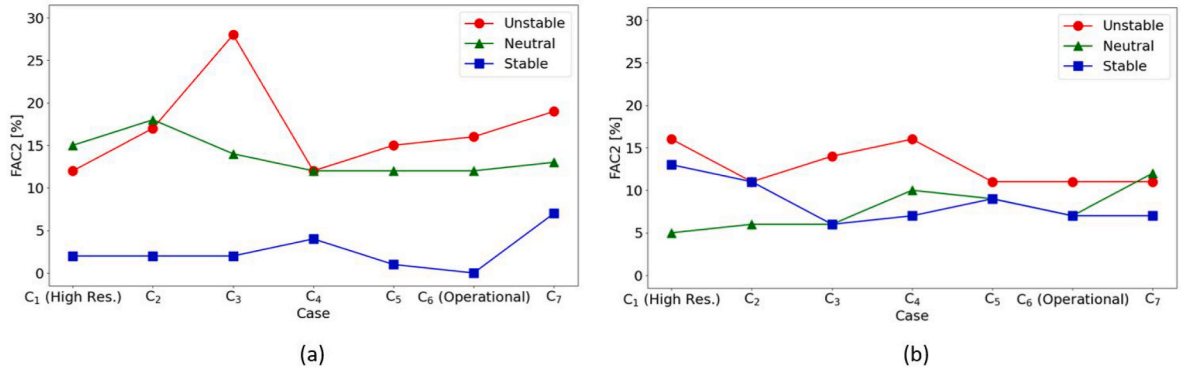

Fig. 8. FAC2 [%] of the surface tracer concentrations predicted by CALPUFF against the CFD-LS values over the different CALPUFF surface station settings and thermal stability conditions for the shallow (a) and deep (b) mine configurations.

the shallow mine configuration under the thermally unstable condition was the only scenario showing sensitivity to the CALPUFF weather station settings. Only here did we find a case (C3) that gave a large increase in *FAC*2 percentage compared with other cases. This is a case with a moderate number of receptors inside the mine.

We shift our focus to look at how well the wind fields calculated in CALMET recreate the CFD flow fields. Fig. 9 shows the calculated Bias [m s^{-1}] and RMSE [m s^{-1}] of horizontal wind speeds at discrete receptors located 10 m above the surface both inside and outside of the mine. These particular receptors were not used by CALMET to calculate the wind fields. Under the unstable condition, Bias [m s^{-1}] and RMSE [m s^{-1}] values lower than 2 m s^{-1} are achieved both inside/outside of the shallow/deep mines. However, the error statistics were higher for the neutral and stable conditions, in agreement with a study by Cox et al. (2005) (their Fig. 2), who examined three diagnostic wind models with data from 26 field experiments. Cases C4 and C6 show the effect of changing the number of surface stations outside the mine (by keeping the number of stations inside the mine constant). The effects are more clear particularly for the thermally stable condition, where for the shallow mine, the wind speed Bias [m s^{-1}] and RMSE [m s^{-1}] are decreased by increasing the number of surface stations from four outside the mine (case C6) to 95 outside the mine (case C4). This may be attributed to a more successful wind field interpolation/extrapolation when more observed station data are included. The Bias [m s^{-1}] for the shallow mine does not change for other stability conditions, as far as changing the number of stations outside the mine is concerned. The same trend for reduction of error statistics is not as clear for the deep mine, suggesting that the CALMET model has difficulties in predicting the wind field, even considering the inclusion of more surface station observations. The operational case C6 demonstrates the same level of accuracy compared to the high resolution case C1.

Fig. 10 shows the calculated Bias [m s^{-1}] and RMSE [m s^{-1}] from CALMET against CFD-LS for vertical profiles of wind speed inside and downstream of the mine for different number of surface station cases. Overall, the error statistics are lower for the unstable condition than for the others. Further, increasing the number of stations help reduce the error statistics for the stable condition. This may be attributed to complexity of the flow structure, such as the formation of standing vortices, with skimming flow under the neutral condition and waves under the stable condition (Figs. 7 and 8 in the study of Kia et al. (2021)), which the CALMET model does not predict.

Overall, Figs. 9 and 10 show that the CALMET model can simulate wind components at 10 m above surface better than the entire boundary layer since the Bias [m s^{-1}] and RMSE [m s^{-1}] error statistics are lower at 10 m above surface. This is consistent with previous evaluations in other studies (Chang et al., 2003; Cox et al., 2005; Wang et al., 2008). This may be due to the fact the wind field is only forced by observations at 10 m above surface and not vertical profiles of wind, which have been shown to deviate from the logarithmic profiles in the surface layer theory (e.g. Fig. 10 in Nambiar et al. (2020a) and Fig. 5 in Nahian et al. (2020)).

Fig. 11 shows the calculated MAE [Degree] of wind direction inside and outside of the mine by CALMET against CFD-LS for the receptors at 10 m above surface. The outside mine areas show lower MAE than inside the mine under all stability conditions. The higher MAE inside the mine reflects the more complex flow in the pit compared with the surrounding flat terrain. This is in agreement with the study of Nahian et al. (2020) who predicted horizontal wind circulations inside a shallow mine pit under all stability conditions (their Fig. 7). On another note, wind direction prediction by CALMET provides better results under neutral and unstable conditions than the stable condition, which is in agreement with the study by Cox et al. (2005) (their Fig. 3). It appears that changing the number of forcing stations does not drastically change the error statistics for wind direction.

Fig. 12 shows the model agreement in MAE [Degree] of wind direction on vertical profiles inside and downstream of the mine. Similar conclusions can be drawn here as was done for Fig. 11. However, there are subtle differences. In the configuration of the shallow mine, the MAE [Degree] for wind direction is approximately 20° lower on boundary-layer profiles than near the surface. This may be due to the fact that

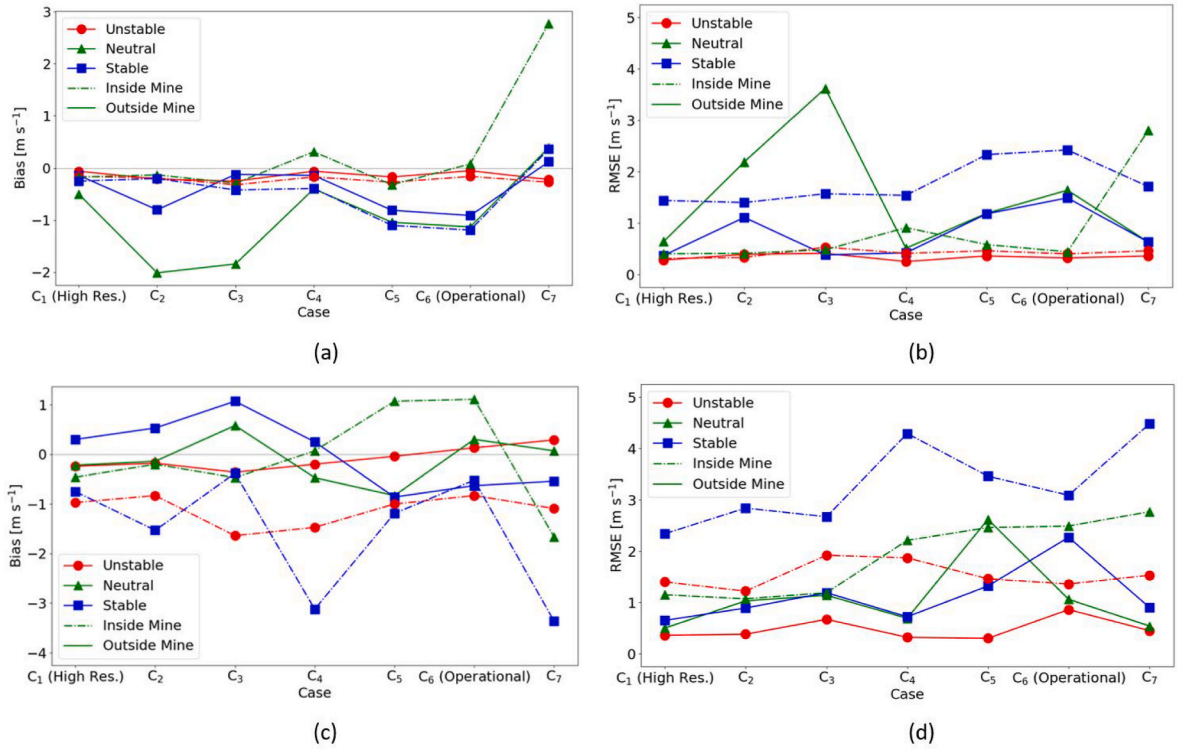

Fig. 9. Bias [m s^{-1}] and RMSE [m s^{-1}] of horizontal wind speed inside and outside of the mine at 10 m above surface, comparing CALMET predictions against CFD-LS over the different surface station cases and thermal stability conditions of the shallow (a and b) and deep (c and d) mine configurations.

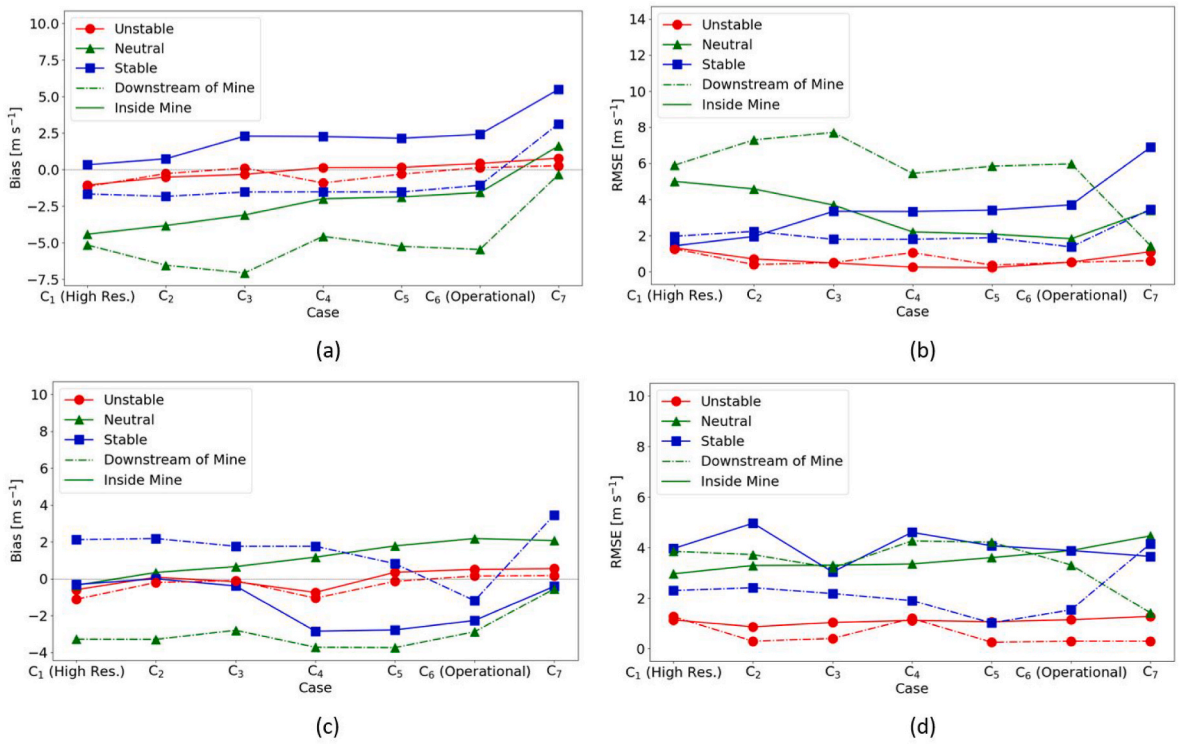

Fig. 10. Bias [m s^{-1}] and RMSE [m s^{-1}] of horizontal wind speed on vertical boundary-layer profiles inside and downstream of the mine predicted by CALMET against CFD-LS over the different surface station cases and thermal stability conditions of the shallow (a and b) and deep (c and d) mine configurations.

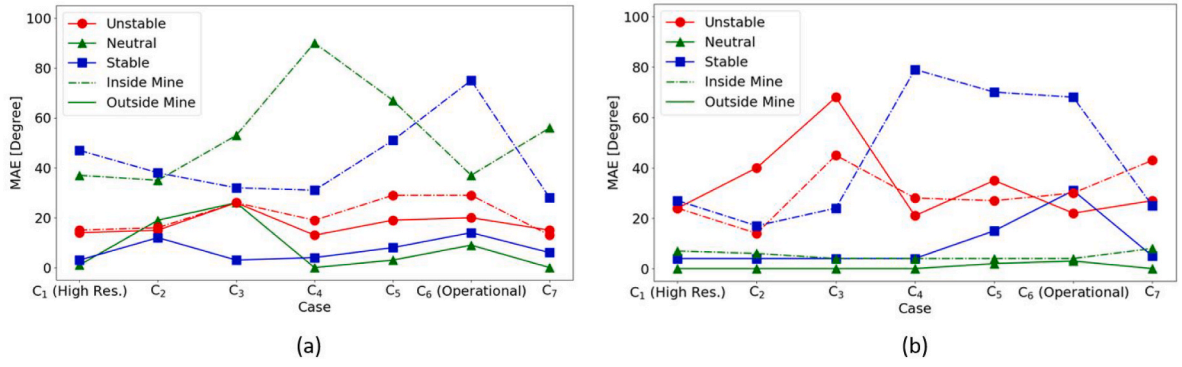

Fig. 11. MAE [Degree] of horizontal wind direction at 10 m above surface inside and outside the mine predicted by CALMET against CFD-LS over the different surface station cases and thermal stability conditions of the shallow (a) and deep (b) mine configurations.

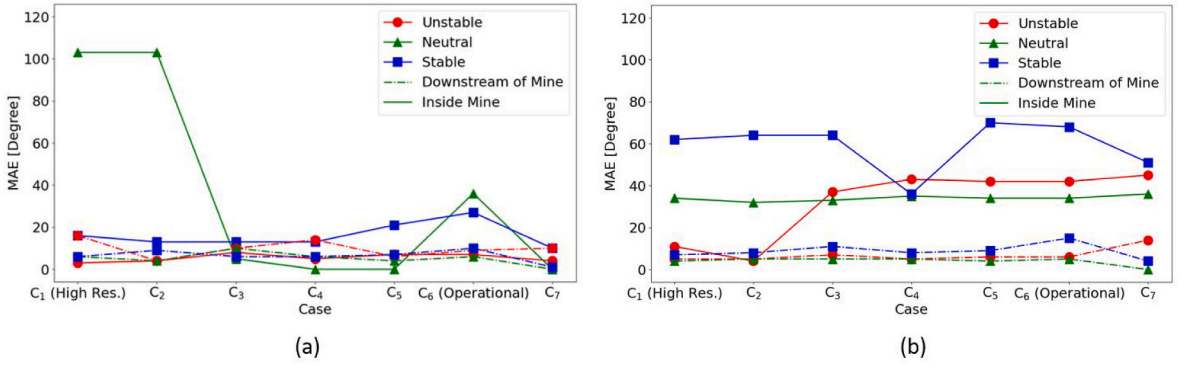

Fig. 12. MAE [Degree] of wind direction on boundary-layer profiles inside and downstream of the mine predicted by CALMET against CFD-LS over the different surface station cases under different thermal stability conditions of the shallow (a) and deep (b) mine configurations.

the effect of topography on wind direction is reduced at higher altitudes. As far as the deep mine is concerned, the influence of the topography on wind direction is present at higher altitudes. For instance, under the stable condition, a standing wave was generated by the deep mine and manifested itself on a substantial portion of the boundary layer in the study of Kia et al. (2021) (their Figs. 7 and 8). Overall, comparing Figs. 11 and 12 show better wind direction prediction on the vertical profiles than near the surface.

Overall, the presented results of concentration and wind field predictions show similar error statistics for the high resolution case C1 and the operational case C6, which demonstrate that increasing the number of surface stations in a diagnostic model does not necessarily result in increased accuracy in the wind and dispersion predictions. This outcome is in agreement with a study by Wang et al. (2008). It appears that interpolation/extrapolation of the wind field by CALMET in this topographically complex environment alone cannot reproduce the complexity predicted by prognostic models such as CFD-LS.

3.2.2. Effect of the location of met stations

Here we consider the sensitivity of the CALPUFF concentration calculations relative to the location of the weather stations used in the CALMET flow calculations. Tables 5 and 6 show the Bias [μg m^{-3}], RMSE [μg m^{-3}], and *FAC*2 [%] of the CALPUFF concentration predictions at the receptors downwind of the mine (at height $z = 10$ m) for case C6 for the shallow and deep mines (the practical operational case). Under the three thermal stability conditions, the error statistics do not change significantly as the surface station locations are changed. We do note that the prediction of plume concentration under the stable and neutral conditions deviate further from the CFD-LS model than under the unstable conditions.

Tables 7 and 8 show the Bias [m s^{-1}] and RMSE [m s^{-1}] of wind speed prediction at different receptors at 10 m above surface inside and outside of the mine and on vertical profiles inside and downstream of the mine by CALMET against CFD-LS for different locations of surface stations and thermal stability conditions for case C6 of the shallow and deep mines. The error statistics change in most of the situations by less than 10% and 25% for near surface and on vertical profiles of the boundary layer, respectively. The tables show that the wind speed prediction is not substantially affected by the location of the surface stations.

Tables 9 and 10 show the MAE [degree] of horizontal wind direction at 10 m above surface inside and outside of the mine and on vertical profiles inside and downstream of the mine predicted by CALPUFF versus CFD-LS for different locations of surface stations and thermal stability conditions for case C6 of the shallow and deep mines. Again, the tables show that the wind direction prediction is not substantially affected by the location of the surface stations.

Table 5
Bias [μg m^{-3}] (RMSE [μg m^{-3}]) of the tracer concentration outside of the mine, predicted by CALPUFF against CFD-LS for different locations of surface stations and thermal stability conditions for case C6 of the shallow and deep mines.

Surface station locations	Bias [μg m^{-3}] (RMSE [μg m^{-3}]) of receptors' concentration outside of the mine					
	Shallow			Deep		
	Unstable	Neutral	Stable	Unstable	Neutral	Stable
$x = 1000$, 8000 [m]	−339 (2749)	−1483 (6871)	5656 (6665)	−195 (1153)	−4347 (7948)	−2557 (3210)
$x = 3000$, 7000 [m]	−361 (2745)	−1250 (6891)	6256 (7093)	−178 (1283)	−4307 (7921)	−2568 (3223)
$x = 3000$, 8000 [m]	−339 (2748)	−1463 (6871)	4863 (5806)	−193 (1152)	−4314 (7930)	−2535 (3211)
$x = 3000$, 9000 [m]	−326 (2749)	−1496 (6851)	5494 (6663)	−221 (1148)	−4347 (7954)	−2553 (3202)

Table 6
*FAC*2 percentage of the tracer concentration, predicted by CALPUFF against CFD-LS for different locations of surface stations and thermal stability conditions for case C6 of the shallow and deep mines.

Surface station locations	*FAC*2 [%] of receptors' concentration					
	Shallow			Deep		
	Unstable	Neutral	Stable	Unstable	Neutral	Stable
$x = 1000$, 8000 [m]	16	12	0	11	7	7
$x = 3000$, 7000 [m]	17	13	0	11	8	9
$x = 3000$, 8000 [m]	19	12	0	11	7	7
$x = 3000$, 9000 [m]	15	12	0	12	8	9

3.2.3. Concentration agreement vs downwind receptor location

In terms of an IDM estimate of emissions, it is valuable to consider if certain locations have lower relative dispersion model errors in estimating $(C/Q)_{\text{sim}}$. If such locations exist, these would be good potential choices for locating the $(C - C_b)$ [μg m^{-3}] measurement for an IDM calculation.

Fig. 13 shows how the Bias [μg m^{-3}] and RMSE [μg m^{-3}] of the CALPUFF surface concentration predictions vary with distance downwind of the mine. For this comparison we group the concentration receptors by their x position. CALPUFF case C6 is used for the comparison. The predictions under all stability conditions show relatively large errors for the receptors close to the mine ($x = 6500$ m). Beyond this distance there is a trend toward reduced Bias [μg m^{-3}] and RMSE [μg m^{-3}] with increasing distance from the mine. This trend exists in all of the configurations (deep and shallow mines) and conditions (thermal stabilities). Perhaps it is no surprise that the CFD-LS and CALPUFF predictions would be most different close to the mine. The mine-pit clearly creates localized flow complexity that would have more of an impact on the plume close to the mine, and would diminish with increasing distance as the ambient ABL becomes re-established. As CALPUFF does not fully replicate the mine-induced complexity indicated by CFD-LS, this should be manifested in near-mine concentrations that are different than CFD-LS.

3.3. Implications

If we accept that the CFD model accurately represents flow complexity in real open-pit mines, then we conclude that CALPUFF modeling of pollutant dispersion from these mines should be performed with caution. In this situation we take CALPUFF-CALMET as being representative of the class of diagnostic models, and we anticipate this conclusion spans the model class. In none of the configurations (mine depths), conditions (thermal stabilities), or cases (CALPUFF setups) studied was there good agreement between the CFD-LS and CALPUFF predictions of the plume concentration downwind of the mine. What do our results say specifically about the potential for calculating mine emission rates using IDM? The most relevant statistic to look at are the *FAC* scores. Over the short-range of downwind distances we studied, the computed *FAC*2 statistic comparing the CALPUFF and CFD-LS concentrations were usually far less than 30% (i.e., surface concentration estimates from the two models were within a factor of two at fewer than 30% of locations). According to Hanna and Chang (2011), this would deem the CALPUFF performance as unacceptable. Because downwind concentration scales on the emission rate for a given source configuration and meteorological conditions, the *FAC* scores for concentration are also the *FAC* scores for an estimate of the emission rate given a $(C - C_b)$ [μg m^{-3}] measurement. Given the *FAC*2 scores we conclude that for the majority of potential $(C - C_b)$ [μg m^{-3}] measurement locations, an

Table 7
Bias [m s^{-1}] (RMSE [m s^{-1}]) of horizontal wind speed inside and outside of the mine at 10 m above surface predicted by CALMET against CFD-LS for different locations of surface stations and thermal stability conditions for case C6 of the shallow and deep mines.

Receptor locations	Surface station locations	Bias [m s^{-1}] (RMSE [m s^{-1}]) of horizontal wind speed					
		Shallow			Deep		
		Unstable	Neutral	Stable	Unstable	Neutral	Stable
Inside mine	$x = 1000, 8000$ [m]	−0.15 (0.40)	0.03 (0.44)	−2.12 (2.42)	−0.83 (1.36)	1.17 (2.50)	−0.48 (2.99)
	$x = 3000, 7000$ [m]	−0.15 (0.40)	−0.16 (0.55)	−1.83 (2.56)	−0.50 (1.37)	1.17 (2.50)	−0.68 (3.03)
	$x = 3000, 8000$ [m]	−0.16 (0.40)	0.08 (0.44)	−2.12 (2.42)	−0.83 (1.36)	1.11 (2.49)	−0.52 (3.09)
	$x = 3000, 9000$ [m]	−0.15 (0.40)	0.04 (0.43)	−2.13 (2.42)	−0.86 (1.38)	1.10 (2.50)	−0.48 (2.99)
Outside mine	x = 1000, 8000 [m]	−0.16 (0.35)	−1.19 (1.66)	−1.30 (1.80)	−0.09 (0.30)	0.79 (1.22)	−0.66 (1.26)
	$x = 3000, 7000$ [m]	−0.08 (0.31)	−1.14 (1.61)	−0.86 (1.32)	−0.15 (0.46)	0.28 (1.05)	−0.97 (1.46)
	$x = 3000, 8000$ [m]	−0.05 (0.32)	−1.13 (1.64)	−0.91 (1.49)	0.13 (0.86)	0.30 (1.06)	−0.63 (2.27)
	$x = 3000, 9000$ [m]	−0.05 (0.39)	−1.40 (1.90)	−1.13 (1.70)	0.01 (0.46)	0.25 (1.00)	−0.49 (1.09)

Table 8
Bias [m s^{-1}] (RMSE [m s^{-1}]) of wind speed on vertical boundary-layer profiles inside and downstream of the mine, predicted by CALMET versus CFD-LS for different locations of surface stations and thermal stability conditions for case C6 of the shallow and deep mines.

Receptor locations	Surface station locations	Bias [m s^{-1}] (RMSE [m s^{-1}]) of wind speed on vertical boundary-layer profiles					
		Shallow			Deep		
		Unstable	Neutral	Stable	Unstable	Neutral	Stable
Inside mine	$x = 1000, 8000$ [m]	0.26 (0.33)	−1.55 (1.89)	2.35 (3.61)	0.53 (1.14)	2.16 (3.85)	−2.27 (3.89)
	$x = 3000, 7000$ [m]	0.38 (0.47)	−1.62 (1.88)	2.37 (3.63)	0.53 (1.17)	2.14 (3.83)	−2.29 (3.91)
	$x = 3000, 8000$ [m]	0.42 (0.53)	−1.56 (1.82)	2.41 (3.70)	0.51 (1.14)	2.18 (3.88)	−2.27 (3.88)
	$x = 3000, 9000$ [m]	0.29 (0.39)	−1.48 (1.79)	2.41 (3.70)	0.47 (1.07)	2.17 (3.81)	−2.29 (3.87)
Downstreammine	$x = 1000, 8000$ [m]	−0.06 (0.40)	−5.4 (5.90)	−1.17 (1.48)	0.14 (0.30)	−2.64 (3.05)	−1.27 (1.62)
	$x = 3000, 7000$ [m]	0.25 (0.63)	−5.94 (6.36)	−1.70 (1.90)	0.19 (0.39)	−2.28 (2.91)	−1.73 (2.15)
	$x = 3000, 8000$ [m]	0.14 (0.52)	−5.45 (5.97)	−1.07 (1.37)	0.15 (0.29)	−2.88 (3.31)	−1.19 (1.53)
	$x = 3000, 9000$ [m]	−0.08 (0.37)	−5.36 (5.90)	−1.14 (1.49)	0.10 (0.26)	−2.00 (3.30)	−1.10 (1.43)

Table 9
MAE [Degree] of horizontal wind direction at 10 m above the surface inside and outside of the mine predicted by CALMET against CFD-LS for different locations of surface stations and thermal stability conditions for case C6 of the shallow and deep mines.

Receptor locations	Surface station locations	MAE [Degree] of horizontal wind direction					
		Shallow			Deep		
		Unstable	Neutral	Stable	Unstable	Neutral	Stable
Inside mine	$x = 1000, 8000$ [m]	29	37	80	30	4	68
	$x = 3000, 7000$ [m]	29	38	61	30	4	69
	$x = 3000, 8000$ [m]	29	37	75	30	4	68
	$x = 3000, 9000$ [m]	29	37	79	30	4	68
Outside mine	$x = 1000, 8000$ [m]	21	14	18	23	4	28
	$x = 3000, 7000$ [m]	22	8	11	22	2	26
	$x = 3000, 8000$ [m]	20	9	14	22	3	31
	$x = 3000, 9000$ [m]	23	17	13	23	3	37

Table 10
MAE [Degree] of wind direction on boundary-layer profiles inside and downstream of the mine, predicted by CALMET against CFD-LS for different locations of surface stations and thermal stability conditions for case C6 of the shallow and deep mines.

Receptor locations	Surface station locations	MAE [Degree] of horizontal wind direction					
		Shallow			Deep		
		Unstable	Neutral	Stable	Unstable	Neutral	Stable
Inside mine	$x = 1000, 8000$ [m]	7	36	27	42	35	67
	$x = 3000, 7000$ [m]	7	36	25	6	35	67
	$x = 3000, 8000$ [m]	7	36	27	42	34	68
	$x = 3000, 9000$ [m]	8	36	26	42	35	68
Downstream of mine	$x = 1000, 8000$ [m]	6	6	10	6	5	16
	$x = 3000, 7000$ [m]	9	5	8	6	3	33
	$x = 3000, 8000$ [m]	9	6	10	6	5	15
	$x = 3000, 9000$ [m]	6	7	5	5	4	35

estimate of the emission rate using a CALPUFF calculation of $(C/Q)_{sim}$ would be in error by more than a factor of two (assuming the CFD-LS calculations represent a real open-pit mine). In fact, for the large majority of locations the CALPUFF calculation of $(C/Q)_{sim}$ would be in error by more than a factor of 10.

One reason for the discrepancy between the two models is that the

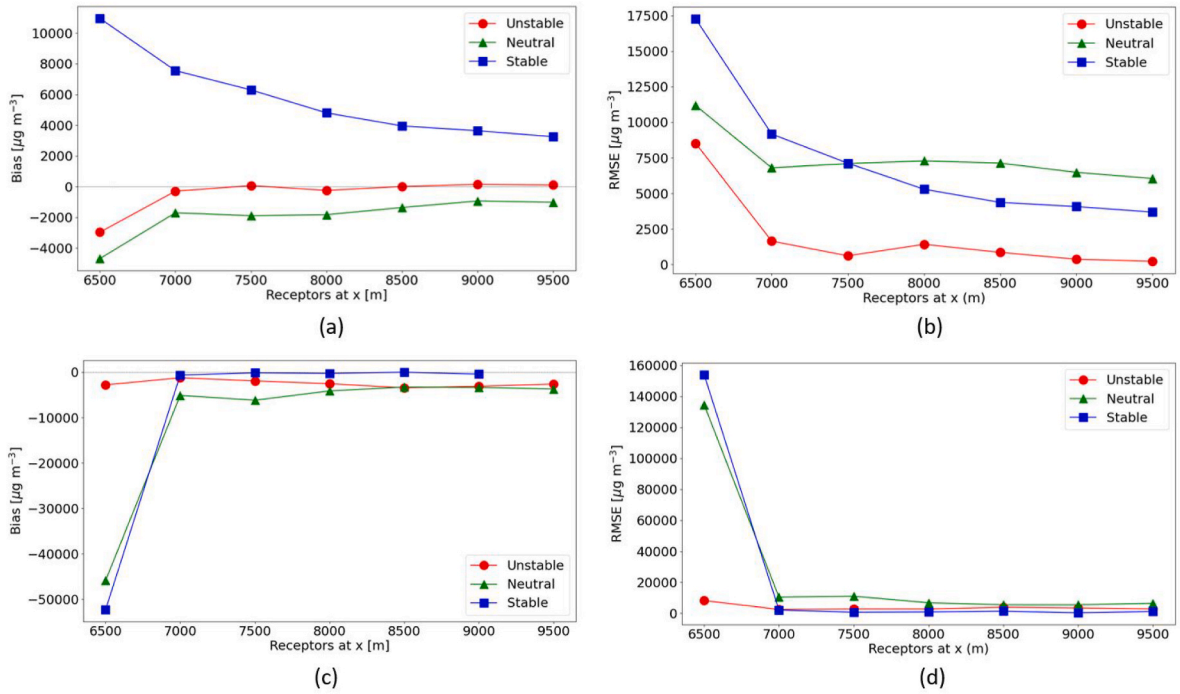

Fig. 13. Bias [$\mu g\ m^{-3}$] and RMSE [$\mu g\ m^{-3}$] of the tracer concentration predicted by CALPUFF against CFD-LS over different receptor locations in the stream-wise direction at 10 m above the surface under different thermal stability conditions of the shallow (a and b) and deep (c and d) mines for case C6.

diagnostically-determined flow field (CALMET), which calculates a flow field by interpolating/extrapolating from a limited set of input wind observations, did not reproduce the complexity of the wind flow in the mine, as indicated by the CFD. It is also likely that the Gaussian modeling approach used in CALPUFF is unable to capture the fine spatial details of the mine plume, which was a pronounced feature of the CFD-LS simulations. Tomasi et al. (2019) and Toscano et al. (2021) showed that CALPUFF simulations tend to generate very uniform patterns, which are not much influenced by the complex topography nor by the complexity of the flow field. They mentioned the poor performance of CALPUFF is associated with its own Gaussian formulation, which prevents the model from capturing the large degree of spatial inhomogeneity in the plume concentration over complex terrains. This capability is a feature of the Lagrangian stocastic approach which is grid-free, and at all scales, it follows the motion of individual tracer particles (Giovannini et al., 2020). Could the CALPUFF calculations of $(C/Q)_{sim}$ be improved? Rather than using the high spatial resolution CFD results to define a limited number of weather stations for use in CALMET, one could use mesoscale models to produce a more complete gridded wind field for input to the CALMET model. Meso-scale models such as WRF and MM5 are operationally simulated with low horizontal resolutions at 2–4 km (Chandrasekar et al., 2003; Jackson et al., 2006; Yim et al., 2010; Gopalaswami et al., 2015; Ruggeri et al., 2020; Tang et al., 2021), which in the present work is the same order as the horizontal dimensions of the mine. This is probably not high enough to resolve the impact of the mine terrain on the flow field, as the effective terrain dimension should be a multiple of the grid resolution (Skamarock, 2004). Such models would be unlikely to represent important features of the wind field associated with the mine, such as vertical and horizontal circulations inside the mine pit. High resolution meso-scale simulations with horizontal grid spacings down to 50–200 m can be performed using the LES method to capture these complex features (Nahian et al., 2020); however, this kind of high-resolution modeling is still beyond reach for operational purposes. In addition, there is evidence that even if high resolution wind fields are provided to CALPUFF, the deficiencies in the Gaussian model still prevents an accurate dispersion prediction (Tomasi et al., 2019; Toscano et al., 2021).

Could an IDM calculation of emissions be based on a CFD-LS simulation? This complex modeling system is unlikely to provide for practical IDM calculations in topographically complex terrain. Our CFD simulations took many days of computation on a computer cluster with 100 CPUs, as well as substantial expertise, to produce results for a single 15-min period. If IDM is to be broadly useable it will likely be paired with more practical diagnostic models like CALPUFF. However, in our specific mine situation (source configuration, ambient wind conditions), a downwind concentration measurement, which is interpreted through a diagnostic model simulation, would give an emission rate far different from that based on CFD-LS. In the large majority of downwind $(C - C_b)$ [$\mu g\ m^{-3}$] measurement locations the two models would give emission rates differing by more than a factor of 10. If one accepts that the CFD-LS model provides a more accurate representation of atmospheric transport in complex terrain than diagnostic models, then one would infer that an IDM approach based on a diagnostic model would be unreliable for open-pit mines. However, one should be cautious about over-generalizing. Would different gas source configurations give different outcomes? For example, would an emission source that covers the total pit surface lead to a more dispersed plume that would be better represented by a diagnostic model? Would non-stationary wind conditions (e.g, mesoscale wind fluctuations) also create a more dispersed plume and increase the accuracy of a diagnostic model simulation? It also seems likely that a CALPUFF emission calculation based on a concentration measurement taken further from the mine (further than the 3 km range studied here) would show greater agreement with the more sophisticated CFD-LS model. A more appropriate conclusion based on this work is that IDM combined with diagnostic dispersion models should be approached with caution in complex terrain.

4. Conclusions and recommendations

Atmospheric transport phenomena were simulated using CALPUFF and CFD-LS models inside and surrounding two synthetic open-pit mines of different depths under different thermal stability conditions. The main aim of the study was to investigate how well the two models compare when predicting wind and concentration fields associated with

dispersion from gas sources in the mine, in order to evaluate the potential for estimating mine emissions using the IDM technique.

Six simulations were conducted for two mine depths: a shallow (100 m) and a deep (500 m) mine and three thermal stability conditions. Overall the CALPUFF surface concentration predictions downwind of the mines are in poor agreement with the CFD-LS predictions. And in most of the configurations the concentration estimates were insensitive to the number and location of meteorological stations used to calculate the wind field in CALPUFF. Overall, less than 30% of receptor points predict the concentration within a factor of two of CFD-LS simulations ($FAC2 < 0.3$). The reasons for the poor CALPUFF agreement are mainly attributed to the complex structure of the flow under such conditions, such as horizontal and vertical wind circulations in the mine, formation of standing waves, and plume rise, which the CALPUFF model cannot predict. It is suggested that the disagreements between the two models are mainly caused by diagnostic modeling of the wind field, versus prognostic modeling, although inaccuracies in the Gaussian puff model may also be possible, which were not investigated in this study.

Diagnostic modeling of wind field and gas dispersion finds many applications in air quality studies and quantification of area-fugitive emission fluxes. There are many examples of successful IDM emission measurements based on these types of models, but the majority have taken place in reasonably simple terrain. The evidence provided in this study shall caution practitioners when using diagnostic tools for investigation of atmospheric transport phenomena related to open-pit mines with complex topography. While the CFD-LS model results are not certain, the findings here can provide guidelines on applicability or appropriate setup for CALPUFF for complex terrains.

Various future recommendations can be provided to improve this work. One of the main drivers of pollutant transport is the wind field, but wind patterns for open-pit mines are not studied in great detail observationally. As the meso-scale models can provide wind field at each grids of the domain in horizontal and vertical directions, it is suggested to use high-resolution meso-scale models to be coupled with CALMET.

The investigation of CALPUFF in this work is not exhaustive. For instance, the investigation of the parameterization of the Gaussian puff model was left out of this study. Also many investigations of parameterizations in the wind field model in CALPUFF can be attempted, such as the interpolation/extrapolation options. In addition, the effect of the horizontal and vertical spatial resolution for forcing the wind field in CALPUFF can be pursued further. Such in depth investigations can be attempted in the future.

All considered, the availability of computational power to predict the wind field and dispersion phenomena using prognostic modeling, such as CFD, high-resolution meso-scale models, or other models, offer a new paradigm for improving wind field and dispersion modeling associated with complex terrains, such as those encountered in open-pit mining areas.

Availability of code and data

The Atmospheric Innovations Research (AIR) Laboratory at the University of Guelph provides the Computational Fluid Dynamics (CFD) model source code. For access, contact Amir A. Aliabadi (aliabadi@uoguelph.ca) or visit http://www.aaa-scientists.com/. Thomas Flesch (thomas.flesch@ualberta.ca) may provide the Lagrangian Stochastic (LS) model.

CRediT authorship contribution statement

Seyedahmad Kia: Data curation, Formal analysis, Investigation, Methodology, Model Comparison, Validation, Visualization, Writing – original draft. **Thomas K. Flesch:** Conceptualization, Data curation, Investigation, Methodology, Supervision, Writing – review & editing. **Brian S. Freeman:** Supervision, Conceptualization, Data curation, Investigation, Methodology, Supervision, Writing – review & editing. **Amir A. Aliabadi:** Conceptualization, Data curation, Formal analysis, Funding acquisition, Investigation, Methodology, Supervision, Writing – review & editing.

Declaration of competing interest

The authors declare that they have no known competing financial interests or personal relationships that could have appeared to influence the work reported in this paper.

Acknowledgments

The authors are indebted to Amanda Sawlor, Datev Dodkelian, Esra Mohamed, Di Cheng, Randy Regan, Margaret Love, and Angela Vuk at the University of Guelph for administrative support. The computational platforms were set up with the assistance of IT staff Jeff Madge, Joel Best, and Matthew Kent at the University of Guelph. Technical guidance from John D. Wilson from University of Alberta, Bahram Gharabaghi from University of Guelph, and Jesse Thé from Lakes Environmental Software is appreciated.

This work was supported by the University of Guelph; the Discovery Grant program (401231) and Alliance program (401643) from the Natural Sciences and Engineering Research Council (NSERC) of Canada; Government of Ontario through the Ontario Centres of Excellence (OCE) under the Alberta-Ontario Innovation Program (AOIP) (053450); and Emission Reduction Alberta (ERA) (053498). OCE is a member of the Ontario Network of Entrepreneurs (ONE). The lead author was partially financially supported by the University of Guelph and Lakes Environmental Software.

References

Ahmadi-Baloutaki, M., Aliabadi, A., 2021. A very large eddy simulation model using a reductionist inlet turbulence generator and wall modeling for stable atmospheric boundary layers. Fluid Dynam. 56, 413–432. https://doi.org/10.1134/S0015462821020026.

Aliabadi, A.A., Krayenhoff, E.S., Nazarian, N., Chew, L.W., Armstrong, P.R., Afshari, A., Norford, L.K., 2017. Effects of roof-edge roughness on air temperature and pollutant concentration in urban canyons. Bound.-Lay. Meteorol. 164, 249–279. https://doi.org/10.1007/s10546-017-0246-1.

Aliabadi, A.A., Moradi, M., Byerlay, R.A.E., 2021. The Budgets of Turbulence Kinetic Energy and Heat in the Urban Roughness Sublayer. Environmental Fluid Mechanics. https://doi.org/10.1007/s10652-021-09800-x.

Aliabadi, A.A., Moradi, M., Clement, D., Lubitz, W.D., Gharabaghi, B., 2019. Flow and temperature dynamics in an urban canyon under a comprehensive set of wind directions, wind speeds, and thermal stability conditions. Environ. Fluid Mech. 19, 81–109. https://doi.org/10.1007/s10652-018-9606-8.

Aliabadi, A.A., Veriotes, N., Pedro, G., 2018. A Very Large-Eddy Simulation (VLES) model for the investigation of the neutral atmospheric boundary layer. J. Wind Eng. Ind. Aerod. 183, 152–171. https://doi.org/10.1016/j.jweia.2018.10.014.

Arregocés, H., Rojano, R., Restrepo, G., Angulo, L., 2016. Using CALPUFF to determine the environmental impact of a coal mine open pit. WIT Trans. Ecol. Environ. 207, 55–66. https://doi.org/10.2495/AIR160061.

Aylor, D.E., Flesch, T.K., 2001. Estimating spore release rates using a Lagrangian stochastic simulation model. J. Appl. Meteorol. Climatol. 40, 1196–1208. https://doi.org/10.1175/1520-0450(2001)040<1196:ESRRUA>2.0.CO;2.

Bahlali, M.L., Dupont, E., Carissimo, B., 2019. Atmospheric dispersion using a Lagrangian stochastic approach: application to an idealized urban area under neutral and stable meteorological conditions. J. Wind Eng. Ind. Aerod. 193, 103976. https://doi.org/10.1016/j.jweia.2019.103976.

Breedt, H.J., Craig, K.J., Jothiprakasam, V.D., 2018. Monin-Obukhov similarity theory and its application to wind flow modelling over complex terrain. J. Wind Eng. Ind. Aerod. 182, 308–321. https://doi.org/10.1016/j.jweia.2018.09.026.

Byerlay, R.A.E., Nambiar, M.K., Nazem, A., Nahian, M.R., Biglarbegian, M., Aliabadi, A. A., 2020. Measurement of land surface temperature from oblique angle airborne thermal camera observations. Int. J. Rem. Sens. 41, 3119–3146. https://doi.org/10.1080/01431161.2019.1699672.

Carter Jr., R.E., Lane, D.D., Marotz, G.A., Chaffin, C.T., Marshall, T.L., Tucker, M., Witkowski, M.R., Hammaker, R.M., Fateley, W.G., Thomas, M.J., et al., 1993. A method of predicting point and path-averaged ambient air VOC concentrations, using meteorological data. Air Waste 43, 480–488. https://doi.org/10.1080/1073161X.1993.10467147.

Chandrasekar, A., Philbrick, C.R., Clark, R., Doddridge, B., Georgopoulos, P., 2003. Evaluating the performance of a computationally efficient MM5/CALMET system for developing wind field inputs to air quality models. Atmos. Environ. 37, 3267–3276. https://doi.org/10.1016/S1352-2310(03)00325-X.

Chang, J.C., Franzese, P., Chayantrakom, K., Hanna, S.R., 2003. Evaluations of CALPUFF, HPAC, and VLSTRACK with two mesoscale field datasets. J. Appl. Meteorol. 42, 453–466. https://doi.org/10.1175/1520-0450(2003)042<0453:EOCHAV>2.0.CO;2.

Clements, C.B., Whiteman, C.D., Horel, J.D., 2003. Cold-Air-Pool structure and evolution in a mountain basin: peter Sinks, Utah. J. Appl. Meteorol. 42, 752–768.

Cox, R.M., Sontowski, J., Dougherty, C.M., 2005. An evaluation of three diagnostic wind models (CALMET, MCSCIPUF, and SWIFT) with wind data from the Dipole Pride 26 field experiments. Meteorol. Appl. 12, 329–341. https://doi.org/10.1017/S1350482705001908.

Fernández-González, S., Martín, M.L., García-Ortega, E., Merino, A., Lorenzana, J., Sánchez, J.L., Valero, F., Rodrigo, J.S., 2018. Sensitivity analysis of the WRF model: wind-resource assessment for complex terrain. J. Appl. Meteorol. Climatol. 57, 733–753. https://doi.org/10.1175/JAMC-D-17-0121.1.

Flesch, T.K., Wilson, J.D., Harper, L.A., Crenna, B.P., 2005. Estimating gas emissions from a farm with an inverse-dispersion technique. Atmos. Environ. 39, 4863–4874. https://doi.org/10.1016/j.atmosenv.2005.04.032.

Flores, F., Garreaud, R., Muñoz, R.C., 2014. OpenFOAM applied to the CFD simulation of turbulent buoyant atmospheric flows and pollutant dispersion inside large open pit mines under intense insolation. Comput. Fluids 90, 72–87. https://doi.org/10.1016/j.compfluid.2013.11.012.

Foken, T., Leuning, R., Oncley, S.R., Mauder, M., Aubinet, M., 2012. Eddy covariance. In: Aubinet, M., Vesala, T., Papale, D. (Eds.), Eddy Covariance. Springer, Dordrecht. https://doi.org/10.1007/978-94-007-2351-1_4.

Giovannini, L., Ferrero, E., Karl, T., Rotach, M.W., Staquet, C., Trini Castelli, S., Zardi, D., 2020. Atmospheric pollutant dispersion over complex terrain: challenges and needs for improving air quality measurements and modeling. Atmosphere 11, 646. https://doi.org/10.3390/atmos11060646.

Gopalaswami, N., Kakosimos, K., Vèchot, L., Olewski, T., Mannan, M.S., 2015. Analysis of meteorological parameters for dense gas dispersion using mesoscale models. J. Loss Prevent. Proc. 35, 145–156. https://doi.org/10.1016/j.jlp.2015.04.009.

Han, X., Liu, D., Xu, C., Shen, W.Z., 2020. Similarity functions and a new $k-\epsilon$ closure for predicting stratified atmospheric surface layer flows in complex terrain. Renew. Energy 150, 907–917. https://doi.org/10.1016/j.renene.2020.01.022.

Hanna, S.R., Chang, J., 2011. Setting acceptance criteria for air quality models. In: Steyn, D.G., Trini Castelli, S. (Eds.), Air Pollution Modeling and its Application XXI. Springer, Dordrecht. https://doi.org/10.1007/978-94-007-1359-8_80.

Hanna, S.R., Chang, J., Strimaitis, D., 1993. Hazardous gas model evaluation with field observations. Atmos. Environ. A. Gen. 27, 2265–2285. https://doi.org/10.1016/0960-1686(93)90397-H.

Jackson, B., Chau, D., Gurer, K., Kaduwela, A., 2006. Comparison of ozone simulations using MM5 and CALMET/MM5 hybrid meteorological fields for the July/August 2000 CCOS episode. Atmos. Environ. 40, 2812–2822. https://doi.org/10.1016/j.atmosenv.2006.01.020.

Joseph, G.M.D., Lowndes, I.S., Hargreaves, D., 2018. A computational study of particulate emissions from Old Moor Quarry, UK. J. Wind Eng. Ind. Aerod. 172, 68–84. https://doi.org/10.1016/j.jweia.2017.10.018.

Kia, S., Flesch, T.K., Freeman, B.S., Aliabadi, A.A., 2021. Atmospheric transport over open-pit mines: the effects of thermal stability and mine depth. J. Wind Eng. Ind. Aerod. 214, 104677. https://doi.org/10.1016/j.jweia.2021.104677.

Kim, H.G., Patel, V., Lee, C.M., 2000. Numerical simulation of wind flow over hilly terrain. J. Wind Eng. Ind. Aerod. 87, 45–60. https://doi.org/10.1016/S0167-6105(00)00014-3.

Li, Y., Guo, H., 2006. Comparison of odor dispersion predictions between CFD and CALPUFF models. T. ASABE 49, 1915–1926. https://doi.org/10.13031/2013.22293.

Liu, X., Cao, J., Xin, D., 2022. Wind field numerical simulation in forested regions of complex terrain: a mesoscale study using WRF. J. Wind Eng. Ind. Aerod. 222 https://doi.org/10.1016/j.jweia.2022.104915, 104915.

Ma, T., Sun, C., 2021. Large eddy simulation of hurricane boundary layer turbulence and its application for power transmission system. J. Wind Eng. Ind. Aerod. 210, 104520. https://doi.org/10.1016/j.jweia.2021.104520.

Medeiros, L.E., Fitzjarrald, D.R., 2014. Stable boundary layer in complex terrain. Part I: linking fluxes and intermittency to an average stability index. J. Appl. Meteorol. Climatol. 53, 2196–2215. https://doi.org/10.1175/JAMC-D-13-0345.1.

Medeiros, L.E., Fitzjarrald, D.R., 2015. Stable boundary layer in complex terrain. Part II: geometrical and sheltering effects on mixing. J. Appl. Meteorol. Climatol. 54, 170–188. https://doi.org/10.1175/JAMC-D-13-0346.1.

Meyers, T.P., Hall, M.E., Lindberg, S.E., Kim, K., 1996. Use of the modified Bowen-ratio technique to measure fluxes of trace gases. Atmos. Environ. 30, 3321–3329. https://doi.org/10.1016/1352-2310(96)00082-9.

Nahian, M.R., Nazem, A., Nambiar, M.K., Byerlay, R., Mahmud, S., Seguin, A.M., Robe, F. R., Ravenhill, J., Aliabadi, A.A., 2020. Complex meteorology over a complex mining facility: assessment of topography, land use, and grid spacing modifications in WRF. J. Appl. Meteorol. Climatol. 59, 769–789. https://doi.org/10.1175/JAMC-D-19-0213.1.

Nambiar, M.K., Byerlay, R.A.E., Nazem, A., Nahian, M.R., Moradi, M., Aliabadi, A.A., 2020a. A Tethered Air Blimp (TAB) for observing the microclimate over a complex terrain. Geoscientific Instrumentation, Methods, and Data Systems 9, 193–211. https://doi.org/10.5194/gi-9-193-2020.

Nambiar, M.K., Robe, F.R., Seguin, A.M., Endsin, M., Aliabadi, A.A., 2020b. Diurnal and seasonal variation of area-fugitive methane advective flux from an open-pit mining facility in northern Canada using WRF. Atmosphere 11, 1227. https://doi.org/10.3390/atmos11111227.

Neophytou, M., Gowardhan, A., Brown, M., 2011. An inter-comparison of three urban wind models using Oklahoma City Joint Urban 2003 wind field measurements. J. Wind Eng. Ind. Aerod. 99, 357–368. https://doi.org/10.1016/j.jweia.2011.01.010.

Peng, X., Lu, G.R., 1995. Physical modelling of natural wind and its guide in a large open pit mine. J. Wind Eng. Ind. Aerod. 54–55, 473–481. https://doi.org/10.1016/0167-6105(94)00060-Q.

Raupach, M., 1989. A practical Lagrangian method for relating scalar concentrations to source distributions in vegetation canopies. Q. J. Roy. Meteorol. Soc. 115, 609–632. https://doi.org/10.1002/qj.49711548710.

Raupach, M.R., Antonia, R.A., Rajagopalan, S., 1991. Rough-wall turbulent boundary layers. Appl. Mech. Rev. 44, 1–25. https://doi.org/10.1115/1.3119492.

Ren, H., Laima, S., Chen, W.-L., Zhang, B., Guo, A., Li, H., 2018. Numerical simulation and prediction of spatial wind field under complex terrain. J. Wind Eng. Ind. Aerod. 180, 49–65. https://doi.org/10.1016/j.jweia.2018.07.012.

Rotach, M.W., Zardi, D., 2007. On the boundary-layer structure over highly complex terrain: key findings from map. Q. J. Roy. Meteorol. Soc. 133, 937–948. https://doi.org/10.1002/qj.71.

Ruggeri, M., Lana, N., Altamirano, J., Puliafito, S., 2020. Spatial distribution, patterns and source contributions of POPs in the atmosphere of Great Mendoza using the WRF/CALMET/CALPUFF modelling system. Emerg. Contam. 6, 103–113. https://doi.org/10.1016/j.emcon.2020.02.002.

Scire, J.S., Strimaitis, D.G., Yamartino, R.J., 2000. A User's Guide for the CALPUFF Dispersion Model (Version 5). Technical Report Earth Tech, Inc. Concord.

Seibert, P., 1999. Inverse modelling of sulfur emissions in Europe based on trajectories. Geophys. Monog. Ser. 114, 147–154.

Skamarock, W.C., 2004. Evaluating mesoscale NWP models using kinetic energy spectra. Mon. Weather Rev. 132, 3019–3032. https://doi.org/10.1175/MWR2830.1.

Streichenberger, B., Chakir, R., Jouy, B., Waeytens, J., 2021. Simulation and Validation of CFD turbulent airflow at pedestrian level using 3D ultrasonic anemometer in the controlled urban area "Sense-City". J. Wind Eng. Ind. Aerod. 219, 104801. https://doi.org/10.1016/j.jweia.2021.104801.

Tang, S., Huang, S., Yu, H., Gu, M., Tang, J., 2021. Impact of horizontal resolution in CALMET on simulated near-surface wind fields over complex terrain during Super Typhoon Meranti (2016). Atmos. Res. 247, 105223. https://doi.org/10.1016/j.atmosres.2020.105223.

Tomasi, E., Giovannini, L., Falocchi, M., Antonacci, G., Jiménez, P.A., Kosovic, B., Alessandrini, S., Zardi, D., Delle Monache, L., Ferrero, E., 2019. Turbulence parameterizations for dispersion in sub-kilometer horizontally non-homogeneous flows. Atmos. Res. 228, 122–136. https://doi.org/10.1016/j.atmosres.2019.05.018.

Toscano, D., Marro, M., Mele, B., Murena, F., Salizzoni, P., 2021. Assessment of the impact of gaseous ship emissions in ports using physical and numerical models: the case of naples. Build. Environ. 196, 107812. https://doi.org/10.1016/j.buildenv.2021.107812.

Wang, W., Shaw, W.J., Seiple, T.E., Rishel, J.P., Xie, Y., 2008. An evaluation of a diagnostic wind model (CALMET). J. Appl. Meteorol. Climatol. 47, 1739–1756. https://doi.org/10.1175/2007JAMC1602.1.

Whiteman, C.D., Haiden, T., Pospichal, B., Eisenbach, S., Steinacker, R., 2004. Minimum temperatures, diurnal temperature ranges, and temperature inversions in limestone sinkholes of different sizes and shapes. J. Appl. Meteorol. 43, 1224–1236. https://doi.org/10.1175/1520-0450(2004)043<1224:MTDTRA>2.0.CO;2.

Wilson, J., Flesch, T., Bourdin, P., 2010. Ground-to-air gas emission rate inferred from measured concentration rise within a disturbed atmospheric surface layer. J. Appl. Meteorol. Climatol. 49, 1818–1830. https://doi.org/10.1175/2010JAMC2427.1.

Wilson, J., Thurtell, G., Kidd, G., Beauchamp, E., 1982. Estimation of the rate of gaseous mass transfer from a surface source plot to the atmosphere. Atmos. Environ. 16, 1861–1867. https://doi.org/10.1016/0004-6981(82)90374-2.

Wilson, J., Yee, E., Ek, N., d'Amours, R., 2009. Lagrangian simulation of wind transport in the urban environment. Q. J. Roy. Meteorol. Soc. 135, 1586–1602. https://doi.org/10.1002/qj.452.

Xia, Z., Cheng, Z., Han, X., Mao, J., 2020. VLES turbulence modelling for separated flow simulation with OpenFOAM. J. Wind Eng. Ind. Aerod. 198, 104077. https://doi.org/10.1016/j.jweia.2019.104077.

Yim, S.H., Fung, J.C., Lau, A.K., 2010. Use of high-resolution MM5/CALMET/CALPUFF system: SO_2 apportionment to air quality in Hong Kong. Atmos. Environ. 44, 4850–4858. https://doi.org/10.1016/j.atmosenv.2010.08.037.

You, Y., Staebler, R.M., Moussa, S.G., Beck, J., Mittermeier, R.L., 2021. Methane emissions from an oil sands tailings pond: a quantitative comparison of fluxes derived by different methods. Atmos. Meas. Tech. 14, 1879–1892. https://doi.org/10.5194/amt-14-1879-2021.

Zhou, T., Yang, Q., Yan, B., Deng, X., Yuan, Y., 2022. Detached Eddy Simulation of Turbulent flow fields over steep hilly terrain. J. Wind Eng. Ind. Aerod. 221, 104906. https://doi.org/10.1016/j.jweia.2022.104906.